This document includes:

1. Point-to-point response to the first reviewer

2. Point-to-point response to the second reviewer

3. List of the major changes in the manuscript

4. Marked-up manuscript
    - changed sections with regard to the comments by reviewer 1 are marked in yellow
    - changed sections with regard to the comments by reviewer 2 are marked in orange
    - changed sections with regard to comments by both reviewers are marked in gray
    - changes with regard to no comments but which serve a better understanding and an improvement of the manuscript are marked in green

Reply to the comments of Reviewer No. 1

Annette Claudia Klein on behalf of the authors
IAG, University of Stuttgart

March 31, 2018

The authors would like to thank the reviewer for his/her efforts and constructive comments. They are very much appreciated and incorporated into the revised manuscript.

In this document the comments given by the 1st reviewer are addressed consecutively. The following formatting is chosen:

- The reviewer comments are marked in blue and italic.
- The reply by the authors is in black color.
- A marked-up manuscript is added. Changed sections with regard to the comments by reviewer 1 are marked in yellow. Changed sections with regard to comments by both reviewers are marked in gray. Changes with regard to no comments but which serve a better understanding and an improvement of the submission are marked in green.

Some manuscripts, which were accepted during the review of this manuscript, are now published:
Fischer et al. 2016 is now referred under Fischer et al. 2018
Wendler et al. (2016) is now published.
Klein et al. (2017) is now referred under Klein et al. (2018)

Moreover, Jost (2017) and Klein (2017) are now replaced by Jost et al. (2018)
The display of the references were adopted in the reference list.

We would like to mention, that since the first submission of this manuscript in September 2017, two conference papers, which partly use the same data as in the present manuscript, were written, submitted and accepted for the AIAA 2018 Conference Series. As these papers reference on the present submission, they were not cited here.

Bartholomay, Sirko, et al. "Towards Active Flow Control on a Research Scale Wind Turbine Using PID controlled Trailing Edge Flaps." 2018 Wind Energy Symposium. 2018.

Marten, David, et al. "Numerical and Experimental Investigation of Trailing Edge Flap Performance on a Model Wind Turbine." 2018 Wind Energy Symposium. 2018.

General comments "G"

1. "*In general, I find the text not always clear, unstructured, and in many cases too vague. The lack of structure makes the text confusing to read, especially because the paper is investigation*

many different parameters, such as experiments, two different numerical codes, blockage effects and the effect of yaw misalignment."

The authors apologize for the inconvenience. In addition to the major and minor comments, the manuscript was completely revised and the authors improved the structure by putting subsection 2.5 into an extra section (Section 3), see **R1:G1** (page 13, line 280).

2. "*Although the results are very interesting, the discussion is not thorough enough and the conclusions oversimplified.*"

The discussion of the results (section 4) was detailed and more specific conclusions were drawn (section 5) in the revised manuscript. More detailed references can be found in the corresponding comments, e.g. Ma3.4, Ma4 or Ma10.

3. "*The differences between the experimental and numerical inflow conditions are neglected. However, the inflow conditions show a difference in the mean velocity of +- 10% compared to the simulation conditions, which seems not negligible. The authors should discuss the consequences of the different inflow conditions on the measurements in more detail.*"

Due to the wind tunnel, the inflow in the experiment is less uniform compared to the simulations and a difference of -10% occurs in a small region, compare **R1:G3** (page 18, line 396). But as the average inflow velocity is the same within the rotor area, the differences in the inflow are lower than $\pm 10\%$. Downstream of the rotor, the differences are bigger, especially in the wake of the nacelle and in the area of the tip vortices, compare Fig. 11. According to Major Comment Ma3.4 and Ma6, and to Major Comment Ma4 and Ma7 of reviewer 2, additional information were added and the consequences were discussed, for example in Table 5 and in Table 6.

4. "*Furthermore, it would be interesting to verify and discuss specifically which physics are modelled correctly by the codes, and which not. For example, one could verify this by estimating the angle of attack, on-blade velocity, and bending moment with a simple BEM method, to verify the benefits of the Lifting Line Free Vortex Wake code.*"

The authors didn't estimate the angle of attack, on-blade velocity, and bending moment with a simple BEM method but prefer to describe the advantages of the vortex codes over traditional BEM methods in the revised manuscript. Moreover, references about the advantages, especially in unsteady operating conditions, were added, compare **R1:G4** (page 9, line 200).
The modelled physics are mentioned with regard to Major Comment Ma10.

5. "*However, the comparison for the bending moment, which is a result of the former two parameters, shows a surprisingly large difference. It would be interesting to discuss the possible causes for this difference in more detail.*"

The authors agree that a discussion of possible causes would be interesting. However, according to the suggestion of reviewer 2 (Ma2), the measured bending moments were removed from the present manuscript because of the large fluctuations and the need of strong filtering, which influenced the bending moments considerably. See also Major Comment Ma8.

Major comments "Ma"

1. "*The introduction does not clearly motivate the research objectives with a literature overview. For instance on page 2, lines 13-15, it is mentioned that earlier studies already verified the effect of wind tunnel walls and blockage effects with simulations. What where the conclusions? From the introduction it is thus unclear what this paper will contribute to the study of wind tunnel blockage effects.*"

The introduction was completely revised.
The objective concerning the influence of the walls on the results was reformulated in the abstract, see **R1:Ma1-b** (page 1, line 3) and in the introduction, compare **R1:Ma1-e** (page 3, line 65)). As the reviewer noted, the effect of the wind tunnel walls were already verified and estimated in other papers (Fischer et al. (2018), Klein et al. (2017)). The conclusions of these papers were now added in the present manuscript, see **R1:Ma1-a** (page 3, line 58). However, the published papers concerning the blockage effect present pure numerical results. No comparisons with experimental data to validate the simulated effect were done, see **R1:Ma1-c** (page 3, line 62). So in the present submission, the gain in knowledge is on the one hand the estimation of the influence assessed with FLOWer, see **R1:Ma1-e** (page 3, line 65). On the other hand, in QBlade, the walls were not taken into account. Therefore, after the validation of the influence of the wind tunnel walls in FLOWer, these simulations can be used for a comparison with FLOWer far field simulations to estimate the effect of the walls, see **R1:Ma1-d** (page 33, line 618). Afterwards, a comparison with the QBlade results can be done. Without the link with FLOWer, a comparison of the experimental results and the simulated QBlade results would not be that meaningful. But with the influence of the wind tunnel estimated, the different results can be compared and interpreted.
Moreover, the literature overview was extended. As suggested by reviewer 2, articles from research groups from JHU, EPFL and KU-Leuven have been taken into account. References about hot-wire measurement to investigate the wake under different operating conditions like yaw misalignment can be found at **R1:Ma1-j** (page 1, line 22). Further information about the measurement of mean velocity and turbulence intensity was integrated at **R1:Ma1-f** (page 2, line 25). References about further applications and benefits of wind tunnels can now be found at **R1:Ma1-g** (page 2, line 31). References about the investigation of the blockage ratio were added at **R1:Ma1-h** (page 2, line 43) and **R1:Ma1-i** (page 2, line 49).

2. "*When a comparison with measurements is done, it is important to consider the measurement uncertainty. Add an estimation of the measurement uncertainty.*"

The velocity planes are measured with hot-wire probes. These probes were calibrated using a KIMO L-type pitot tube with an error of 1% corresponding to 0.1 m/s at the maximum calibrated velocity. The dynamic pressure was measured using a Baratron (pressure sensor) with an error of 0.15% of the pressure reading. The latter corresponds to a velocity error of 0.07% = 0.0075 m/s at the maximum calibrated velocity. Therefore, the error due to the calibration error is 0.1075 m/s. In order to assess the bias error between the probes, in all measurements of the campaign, a set of 20 measurement positions was measured by each probe. Thereby, the bias between the probes was determined. The maximum bias of the probes was determined from the entire dataset as 0.33 m/s, corresponding to 3.3% in reference to maximum calibrated velocity of 10m/s. This is in good agreement to the error estimation shown in the Dantec User Guide, Finn (2002), where the velocity error is calculated to 3%. Summarizing, the error due to calibration and the hot-wire measurement chain is 4.37%, corresponding to 0.44 m/s.
This information is now added in the manuscript, see **R1:Ma2-b** (page 14, line 297).
Moreover, the simulated and measured averaged standard deviation for the velocity planes can now be found in Table 5 and Table 6 and values are now mentioned and discussed in the text, see **R1:Ma2-i** (page 17, line 387) and **R1:Ma2-j** (page 19, line 423).
The on-blade velocity and angle of attack are measured by three-hole probes on the rotor blade. In order to assess the error of these measurements, the measurement chain was analyzed. The three-hole probes were separately (detached from the rotor blade) calibrated in a calibration-setup. The relative error for the velocity measurement amounts 1% in reference to the maximum speed of 22 m/s, which corresponds to 0.22 m/s. In a range of -30deg to +30deg,

the maximum error (bias) for the AoA is 1.6%/Fullscale, which corresponds to 0.48deg for the considered velocity range. To assess the error of the induction correction, the probe was installed in a 2d-wing setup, which ist mounted on a turn table. Thereby, the velocity was compared also to the inflow velocity, that was measured by a differential pressure measurement along the duct section upstream of the test-section. An error of 2%-2.7% is present in the linear region, corresponding to an error of 0.3 to 0.4 m/s. The calculated AoA are compared to the AoA that is set by the turn-table. Within the linear attached flow region, the error of the AoA measurement remains below 2% in reference to the 40deg pitched airfoil, which corresponds to 0.8deg. As the error for the induction correction includes the error which is created by a 'pure' three-hole probe setup, the maximal errors of the velocity and AoA measurement can be summarized for the linear attached flow region as $\Delta AoA = 0.8deg$ and $\Delta v = 0.4m/s$.
This information is now added in the manuscript, see **R1:Ma2-a** (page 15, line 329).
Moreover, information about the average standard deviation of the measured on-blade velocity is now mentioned in the text, see **R1:Ma2-c** (page 21, line 451), **R1:Ma2-d** (page 22, line 476) and **R1:Ma2-e** (page 24, line 493). The averaged standard deviation for the measured AoA was added as well, see **R1:Ma2-f** (page 25, line 512), **R1:Ma2-g** (page 26, line 542) and **R1:Ma2-h** (page 29, line 562).

3. "*Section 2 about the 'methodology and setups' is badly organized and needs a significant improvement.*"

The manuscript was reorganized to improve the structure. About the methodology and setups, the general information about the setups were now placed at the beginning, see **R1:Ma3-a** (page 4, line 90). Afterwards, the different setups are described, starting with the experimental setup. Thereby, the order was from big (wind tunnel) over turbine to small (blade). The description of the two numerical codes starts with information about the code, which is in each case followed by the description of the numerical setup used for the present submission. Afterwards, the data acquisition is introduced with Fig. 6, see **R1:Ma3-b** (page 13, line 281).

3.1 "*Each section and sub-section needs an introduction.*"

An overall introduction for the whole section as well as short descriptions of the content of each subsection were added, see **R1:Ma3.1-a** (page 3, line 86), **R1:Ma3.1-b** (page 4, line 90), **R1:Ma3.1-c** (page 5, line 106), **R1:Ma3.1-d** (page 8, line 176), **R1:Ma3.1-e** (page 10, line 223) and **R1:Ma3.1-f** (page 13, line 280).

3.2 "*The section about the wind tunnel is too short and brief.*"

The section about the wind tunnel is now more detailed. The authors added more information about the wind tunnel and the composition of the test section which could be helpful to understand the present setup, see **R1:Ma3.2-a** (page 5, line 111) and **R1:Ma3.2-b** (page 5, line 115). Further information about the inflow was added in the course of the consideration of Ma3.4.

3.3 "*It is not necessary to mention the top-speed for the wind tunnel test section which is not used in this paper.*"

The information was removed, see **R1:Ma3.3-a** (page 5, line 111) and **R1:Ma3.3-b** (page 5, line 116).

3.4 "*The measurements are performed in the settling chamber which has as purpose to condition the non-homogeneous and turbulent flow from the wind tunnel fan before it enters the test section. As figure 9 indicates, there is a significant mean shear over the cross section in the settling chamber, and the turbulence intensity is not negligible. It is important to provide*

a motivation for this configuration, provide a characterization of the inflow and turbulence properties, and discuss the effects it may have on the results."

A motivation for this configuration was added, see **R1:Ma3.4-a** (page 5, line 111).
Information about the velocity plane and the occurring inequality were investigated by Bartholomay et al., 2017, and were addressed in Subsection 4.1, see **R1:Ma3.4-c** (page 16, line 373).
More information about the distribution of the turbulence intensity were added, see **R1:Ma3.4-b** (page 5, line 118).
Additionally, the authors included tables with the streamwise mean velocity, the standard deviation of the streamwise velocity as well as the global turbulence intensity in x-y-direction for both locations, see Table 5 **R1:Ma3.4-f** (page 17, line 383) and Table 6 **R1:Ma3.4-g** (page 19, line 418). Moreover, the mean differences between measurement and simulation were determined and mentioned in the text, see **R1:Ma3.4-h** (page 18, line 395) and **R1:Ma3.4-i** (page 20, line 430).
An overview on the influence of the turbulent inflow on the results was added, see **R1:Ma3.4-d** (page 5, line 122) and was already given in Section 4, see **R1:Ma3.4-j** (page 19, line 406), **R1:Ma3.4-k** (page 19, line 410) and **R1:Ma3.4-l** (page 21, line 445). The authors want to remark, that for the present investigations, which are a basis for the subsequent investigations of the wind turbine including flaps, the focus was not on the exact reproduction of the unsteady inflow conditions. This will be done in future investigations and is now mentioned in the manuscript, see **R1:Ma3.4-e** (page 18, line 392).

3.5 "*Section 2.1 'Experimental setup' does not describe the velocity measurement setup.*"

The velocity measurement setup was already described in sub-subsection 3.1 together with the description of the approach for the FLOWer simulations, see **R1:Ma3.5** (page 13, line 286). The authors preferred to put the descriptions of the data acquisition for experiment and simulations in one subsection rather than divide them into different subsections.

3.6 "*Mention the specific acquisition devices, and not just the name of the manufacturer.*"

Specific acquisition devices can now be found at **R1:Ma3.6-a** (page 8, line 150), **R1:Ma3.6-b** (page 8, line 151) and **R1:Ma3.6-c** (page 8, line 162).

4. "*P5 Figure 3: The actuators for the flaps and the 3-hole probes + air tubes on the smart blade look like they will influence the airflow around the blade. The presence and impact of this blockage should be discussed.*"

Information about the influence of the probes, their holder and the tubing was added, see **R1:Ma4-a** (page 8, line 164). Moreover, a reason for the neglect in the simulation was added, too, see **R1:Ma4-b** (page 13, line 271).

5. "*P10 L3: An acquisition time of 16 seconds is short for velocity measurements. Please motivate, e.g. based on the integral time scale, that this is sufficiently long for good statistics.*"

The time is assumed to be long enough for good statistics for the current setting as the measured integral length scale is $\leq 0.15m$. With the inflow velocity of 6.5m/s as convective velocity, an integral time of t = 0.15m / 6.5m/s = 0.023s is achieved, which is considerably smaller than the acquisition time of 16s. This information was added in the manuscript, see **R1:Ma5** (page 14, line 289).

6. "*P15 L5: I don't agree with the statement that the error is small. The error in figure 12 is higher than 10% in a large part of the wake: shear region and center.*"

Fig. 12 in the first submission corresponds to Fig. 11 in the present submission.
The authors agree and reformulated the sentence see **R1:Ma6-a** (page 20, line 429). Moreover, the wording "quite good" was replaced with "acceptable", see **R1:Ma6-b** (page 21, line 436). Additionally, as already mentioned in relation to Major Comment Ma3.4, the mean differences between measurement and simulation were determined and mentioned in the text, see **R1:Ma3.4-h** (page 18, line 395) and **R1:Ma3.4-i** (page 20, line 430).

7. "*Figure 18: The experiments show a significant dip around 90 degrees. This is not visible in the simulations. Is there a reason for this effect? Is this also due to the traverse? Explain the situation.*"

This effect is also due to the traverse, which was located upstream of the rotor during all measurements. The influence of the traverse is now mentioned for CaseYAW15, see **R1:Ma7-a** (page 26, line 537), and CaseYAW30, too, see **R1:Ma7-b** (page 28, line 554).

8. "*The differences between the measured and simulated bending moments in figures 20 and 21 are significant. It is not ok to say that this is a good agreement. The experimental curves follow a different pattern, especially for CaseBase. Is there an explanation for this?*"

The authors agree, that the differences between the measured and simulated bending moments are significant.
Strong fluctuations are visible in the raw data of the measured bending moments and heavy filtering was necessary to obtain the distributions shown in the first version of this manuscript. The resulting data should only be used for qualitative comparison to numerical results but cannot be considered as valid basis for quantitative comparisons and code validation purposes. We therefore decided, based on Major Comment Ma2 for reviewer 2, to discard all measured bending moments in the revised version of the manuscript.
The reason for the removal is given at **R1:Ma8-a** (page 16, line 351) and the text was adopted and the corresponding passages were removed, see **R1:Ma8-b** (page 1, line 12), **R1:Ma8-c** (page 1, line 13), **R1:Ma8-d** (page 3, line 80), **R1:Ma8-e** (page 29, line 569), **R1:Ma8-f** (page 30, line 582), **R1:Ma8-g** (page 31, line 590), **R1:Ma8-h** (page 33, line 639), **R1:Ma8-i** (page 33, line 644) and **R1:Ma8-j** (page 33, line 646). The corresponding figures (Fig. 19 and Fig. 20) were adopted, too.
As one of the objectives is the comparison of a medium and a high fidelity code, we consider a comparison of the bending moments calculated with the two numerical methods important. However, the QBlade results were revised and improved in the course of another paper (Marten et al. 2018). They were replaced in the present manuscript, too, to provide the latest results. In this concerning paper, the present manuscript was cited.
In the former QBlade simulations, the size of the vortex was estimated too large. Instead of the time offset, the parameter "initial vortex core size" is used now in the vortex evolution equation. This parameter is more common in literature and better defined. In the present investigation, approximately 10% midspan chord are used for this parameter, leading to a 50% smaller vortex core. The relevant parameters for the QBlade simulation are now listed in Table 3.
The corresponding Figures (Fig. 19 and Fig.20) were adopted.

9. "*The authors should be careful with copyrights. For instance figure 1a, figure 2, figure 3b and figure 8 can be found identically in the paper 'Reproducible inflow modifications for a wind tunnel mounted research HAWT' by Bartholomay S., et al. 2017.*"

Thanks a lot for this information. The authors are in contact with ASME concerning the copyright. But as the pictures show setups and approaches and no result graphs, it should not

cause an infringement. However, Fig. 3 (former Fig.2) was replaced and Fig. 4 (former Fig. 3b) is slightly changed, to have less identical pictures.
If needed, the pictures can also be completely replaced.

10. "*P24 L26: The main conclusion of this paper is too strong. The experiments have too many differences (e.g. vertical shear and turbulence) to make this statement. Furthermore, the agreement for the bending moment is not good at all. Instead make conclusions on what can be estimated correctly, what not, and which physics are modelled correctly.*"

The conclusion was completely revised and the authors tried to make the conclusion less strong, see **R1:Ma10-a** (page 33, line 623), **R1:Ma10-c** (page 33, line 624), **R1:Ma10-e** (page 33, line 626) and **R1:Ma10-n** (page 33, line 648).
Additionally, we extended the conclusions to quantify the differences between simulation and measurement, see **R1:Ma10-b** (page 33, line 624), **R1:Ma10-d** (page 33, line 625), **R1:Ma10-i** (page 33, line 633) and **R1:Ma10-j** (page 33, line 635) in order to find out, how good the parameters can be estimated.
Moreover, the according reasons for the differences were added, see **R1:Ma10-g** (page 33, line 626) and **R1:Ma10-s** (page 34, line 658)
Furthermore, information about the modelled physics are extended and added, see **R1:Ma10-t** (page 32, line 611), and **R1:Ma10-u** (page 32, line 613) as well as **R1:Ma10-h** (page 33, line 641) and **R1:Ma10-o** (page 33, line 649).

Minor comments "Mi"

1. "*Define abbreviations at first use in the main text. Don't define abbreviations in the abstract, and limit the use of abbreviations in the abstract. For example CFD, LLFVW, URANS, ..*"
The abbrevations are removed from the abstract and inserted at the first use in the main text, see **R1:Mi1-a** (page 1, line 7), **R1:Mi1-b** (page 1, line 8), **R1:Mi1-c** (page 1, line 10), **R1:Mi1-e** (page 1, line 11), **R1:Mi1-f** (page 1, line 11), **R1:Mi1-g** (page 1, line 13), **R1:Mi1-h** (page 2, line 37), **R1:Mi1-i** (page 3, line 72) and **R1:Mi1-j** (page 2, line 54).

2. "*Throughout the text, several sentences are unnecessarily long, or have a structure where the subject is placed at the end, which can be confusing. Improving these sentences will benefit the clarity of the text.*"

The complete manuscript was revised to make the wording more concise.

"*Some examples are:*"
2.1 "*P1, L1*"

The syntax was changed, see **R1:Mi2.1** (page 1, line 1)

2.2 "*P1, L2: This is a long sentence and not entirely clear. For instance 'methods of different fidelity' is too vague.*"

The sentence was cut into several short sentences, see **R1:Mi2.2-a** (page 1, line 2), **R1:Mi2.2-b** (page 1, line 2), **R1:Mi2.2-d** (page 1, line 4) and **R1:Mi2.2-e** (page 1, line 3). Moreover, 'methods of different fidelity' is more specified, see **R1:Mi2.2-c** (page 1, line 5)

2.3 "*P1, L5: Is it relevant where the code was run?*"

The information was inserted to make clear, which part of the data was created at which institution and can therefore be assigned to the authors. We therefore prefer to keep this information.

2.4 "*P2, L3: long sentence.*"

The sentence was reformulated and split into two sentences, compare **R1:Mi2.4-a** (page 3, line 68) and **R1:Mi2.4-c** (page 3, line 69).

3. "*P2 L11: It is not clear what 'a one third model' is + this is a long sentence.*"

Information about the one third model is added and the sentence is splitted into two sentences, see **R1:Mi3-a** (page 2, line 55).

4. "*P2 L17: The yaw angle is negative. Does this matter? The orientation is not mentioned.*"

Due to the revision of the introduction, the sentence was omitted.
However, the word "clockwise" was added at the description of the yaw cases, see **R1:Mi4** (page 4, line 95). In the experiment, the door to the settling chamber would have been blocked if the turbine would have been rotated counter clockwise.

5. "*P2 L19: 'the flow around the rotor' is too vague.*"

Due to the revision of the introduction, the sentence was omitted.

6. "*Define the term 'far field conditions'.*"

A short explanation of what is meant by 'far field condition' is added, see **R1:Mi6** (page 11, line 239).

7. "*Units need to be formatted correctly.*"

The format of the units were changed throughout the whole manuscript. For reasons of simplicity, it is only marked with **R1:Mi7-a** (page 5, line 117) and **R1:Mi7-b** (page 13, line 286) exemplary.

8. "*The first sentence of the introduction is too vague and unnecessary.*"

The first sentence was deleted and the following sentence was adjusted, see **R1:Mi8** (page 1, line 18).

9. "*P1 L17: You mention 'simulations' but the referenced paper presents experimental results.*"

That was an infelicitous wording. The mentioned paper was only a reference for the MEXICO project and not for the simulations of the MEXICO rotor in particular. The authors apologize for the confusion. The sentence was adopted and an exemplary reference for the simulation of the MEXICO experiments was added, see **R1:Mi9-a** (page 2, line 34) and **R1:Mi9-b** (page 2, line 38).

10. "*P2 L16: Instead of 'three different states', it would be more clear to mention 'Three different yaw-misalignment cases'.*"

The sentence was changed, see **R1:Mi10** (page 3, line 76).

11. "*P2 L23: This sentence is very long, consider breaking it up in several more clear and well defined sentences.*"

The sentence was revised and split up in shorter sentences, see **R1:Mi11-a** (page 3, line 64), **R1:Mi11-c** (page 3, line 66) and **R1:Ma1-e** (page 3, line 65).

12. "*P3 L6: The text mentions 'low Reynolds numbers'. Please describe the Reynolds numbers at which the experiments are run, and motivate if the experiments scale realistically.*"

The main goal of the turbine is to deliver data for the comparison to simulations and to test and analyze flow control devices and not to compare the overall performance to a turbine in the free field. Therefore, a low Reynolds airfoil was selected as it provides attached flow in the root region of the turbine, which is better for the comparability of experiment and simulation. Over the whole blade span, the Reynolds number ranges from Re=170000 at 15%R over Re=276000 at 50%R to Re=162000 at 98%R. The Reynolds numbers at 15%R and 75%R are now provided, see **R1:Mi12-c** (page 6, line 133) and Table 2.
The load alleviation concepts will be investigated in future studies and this submission serves as a basis. In the manuscript, additional information concerning the airfoil see **R1:Mi12-a** (page 6, line 132), **R1:Mi12-b** (page 6, line 132) and the motivation of the scaling, see **R1:Mi12-d** (page 6, line 140), were added.

13. "*P3 L9: How is the boundary layer thickness estimated? Is it possible to indicate the tape on figure 3?*"

That was a mistake the authors want to apologize for. The turbulator heights for the model wind turbine were adopted to the Reynolds number, which changes with blade radius. It was estimated with the help of an additional 2D experiment. Thereby, the Reynolds number over the whole blade radius was determined and reproduced in the Model Wind Tunnel (MWT) of the IAG, University of Stuttgart. With the help of a stethoscope, the state of the flow was investigated behind zig-zag tapes with different heights. Based on these investigations, the turbulator heights for the BeRT turbine were estimated in order to get a defined transition position and to avoid overtripping. The sentence was adopted and a short remark, that the heights were estimated experimentally was added in the submission, see **R1:Mi13** (page 6, line 136).
The tape position is now indicated in the corresponding figure (Fig. 4, former Fig. 3).

14. "*P3 L15: It is confusing to mention at this point in the text the overall goal of the research project, as it is different from the objectives of this paper.*"

The sentences was reformulated and refers now to the aims of the manuscript rather than the aims of the overall project, see **R1:Mi14** (page 6, line 145).

15. "*P5 L2: What is meant with 'trailing edge deployment'?*"

The smart blade has trailing edge flaps. The actuators are used to deflect the flaps and the sensors to monitor the deflection. So the word 'flap' was missing and is now added, see **R1:Mi15** (page 8, line 158).

16. "*Table 2: What are the units for the wake length?*"

The wake length is measured in rotor revolutions after release of the respective wake elements. A wake length of two means that a wake element is removed from the domain after the rotor completes two full revolutions after it has been released from the blades trailing edge. Additional information was added in the text, see **R1:Mi16** (page 10, line 216).

17. "*P6 L14: 21 panels are mentioned in the text, but in Table 2 15 panels are mentioned. Which one is correct?*"

The final calculations have been carried out with 21 blade panels. It was corrected in the table, see Table 3 (former Table 2).

18. "*P7 l3: It is not entirely clear what is meant with 'overlapped using the CHIMERA technique', overlapping several grids?*"

The sentence was extended, see **R1:Mi18** (page 11, line 232). And yes, several grids overlapp, as each component of the wind turbine has a separate grid. Afterwards, the single components are put together and the grids are overlapped. The flow of information between the single meshes is handled with the help of the so called Chimera technique. More information about the technique can be found in the corresponding reference. The most important advantages of the technique are the possibility to adopt the mesh for every body to the corresponding requirements of the body and the possibility to move the grids against each other.

19. "*P7 L7: Don't use double brackets '(())'.*"

The double brackets were removed, see **R1:Mi19** (page 11, line 236).

20. "*Table 3: I suppose the units are millions of cells?*"

Yes, that is correct. The information can be found in the table header, but it was now added in first column of Table 4, (former Table 3), too.

21. "*P 8 L6-7: This is a repetition.*"

The sentence was deleted and some of the information are placed in the next sentence, see **R1:Mi21** (page 12, line 248).

22. "*Table 4 is an important table. Maybe it can be discussed earlier in the text.*"

Indeed, the table is important and helps to clarify the different cases. Therefore, the whole subsection including Table (Table 1, former Table 4) is now placed at the beginning of the section, see **R1:Mi22-a** (page 4, line 90) and **R1:Mi22-b** (page 4, line 103). Moreover, the title of the section was changed so its content is more obvious and information about the position of the nozzle were added.

23. "*P10 L3: Which probe was taken as the reference then? How are the hot-wire probes calibrated?*"

The mean value of all four probes was calculated and used as reference for each measurement position. Additional information about the offset correction and the calibration of the probes were added, see **R1:Mi23** (page 14, line 292).

24. "*Figure 7 is unnecessary.*"

The figure was deleted.

25. "*P11 L15: How much are these corrections typically? Maybe indicate in figure 16.*"

The sentence was reformulated in order to make it more understandable. Moreover, an approximated linear equation for the conversion of the local flow angle at the probe to the actual AoA, which is valid in the linear regime, was added, see **R1:Mi25** (page 15, line 323) and equation 1.
The authors preferred this way of displaying the conversion instead of the indication in a figure. Regarding Ma2, additional information about error was added in the revised manuscript, see **R1:Ma2-a** (page 15, line 329).

26. "*P12: The description of the strain gauge setups should be done in the experimental setup section.*"

The strain gauge is now mentioned in the section 2.1.3 , see **R1:Mi26** (page 8, line 168), but no more detailed description is present, as the measured bending moments are no longer part

of the submission.

27. "*P9 L17 The text mentions measurements at 1.05d , while P13 L3 doesn't mention measurements at 1.05D. Be consistent, also with the unit of 'D'.*"

All positions are now designated with a lower-case "d", according to Fig. 2.
The measurements were performed at three positions. Therefore, for reasons of completeness, the authors mentioned in the manuscript. But because of space reasons, only two locations were analyzed in the submission. Moreover, the additional position at 1.05d would not have brought further benefit for the manuscript.
An additional sentence which explains this fact is added, see **R1:Mi27** (page 16, line 364).

28. "*P13 L15 'More information about this topic can be found in..' is too vague.*"

It is now more specified what can be found in the provided reference, see **R1:Mi28** (page 17, line 381).

29. "*P14 L6: 'Some aspects' is too vague.*"

The aspects are now more specified, see **R1:Mi29** (page 18, line 401).

30. "*P14 L10-15: Conclusions on wake comparison are not clear, which of the two simulations is discussed?*"

A sentence is added in subsection 3.1 to make clear, that only the velocity planes from the simulation including wind tunnel are taken into account in the whole submission, see **R1:Mi30-a** (page 14, line 302). Moreover, in the text where the comparison is made, it is also mentioned that the comparison to the simulation including wind tunnel is drawn, see **R1:Mi30-b** (page 19, line 406).

31. "*P15 L12: What does this mean for the measurement blade: isn't 100% the maximal radial position?*"

You are right, 100% is the maximal radial position of the blade, which corresponds to 1.5m and represents the tip. Consequently, 0% corresponds to the center of the rotor. This information is now added, compare **R1:Mi31-a** (page 21, line 441) and **R1:Mi31-b** (page 21, line 442).

32. "*P17 L8-10: 'More information about..' is too vague.*"

The intention of the authors to mention this reference was to give the reader a possible reference, where they can find detailed information about all the effects which occur under yawed inflow. The sentence is now changed, see **R1:Mi32** (page 23, line 488).

33. "*P18 L10: 'More information about..' is too vague.*"

The authors could not explain all the details about the different methods to extract the on-blade velocity and the angle of attack. However we wanted to give information about further literature. The authors now changed the way the reference is mentioned in the text, see **R1:Mi33** (page 26, line 518).

34. "*P18 L13-L16: This should be mentioned in the introduction.*"

The sentences were move in the introduction, see **R1:Mi34-a** (page 2, line 47) and **R1:Mi34-b** (page 2, line 42)

Reply to the comments of Reviewer No. 2

Annette Claudia Klein on behalf of the authors
IAG, University of Stuttgart

March 31, 2018

The authors would like to thank the reviewer for his/her efforts and constructive comments. They are very much appreciated and incorporated into the revised submission.

In this document the comments given by the 2nd reviewer are addressed consecutively. The following formatting is chosen:

- The reviewer comments are marked in blue and italic.
- The reply by the authors is in black color.
- A marked-up manuscript is added. Changed sections with regard to the comments by reviewer 2 are marked in orange. Changed sections with regard to comments by both reviewers are marked in gray. Changes with regard to no comments but which serve a better understanding and an improvement of the manuscript are marked in green.

Some manuscripts, which were accepted during the review of this manuscript, are now published:
Fischer et al. 2016 is now referred under Fischer et al. 2018
Wendler et al. (2016) is now published.
Klein et al. (2017) is now referred under Klein et al. (2018)

Moreover, Jost (2017) and Klein (2017) are now replaced by Jost et al. (2018)
The display of the references were adopted in the reference list.

We would like to mention, that since the first submission of this manuscript in September 2017, two conference papers, which partly use the same data as in the present manuscript, were written, submitted and accepted for the AIAA 2018 Conference Series. As these papers reference on the present submission, they were not cited here.

Bartholomay, Sirko, et al. "Towards Active Flow Control on a Research Scale Wind Turbine Using PID controlled Trailing Edge Flaps." 2018 Wind Energy Symposium. 2018.

Marten, David, et al. "Numerical and Experimental Investigation of Trailing Edge Flap Performance on a Model Wind Turbine." 2018 Wind Energy Symposium. 2018.

General comments "G"

1. "*Unfortunately, the paper suffers from major issues that require a major revision before the paper can be considered for the publication.*"

The authors apologize. The manuscript was completely revised and all comments were considered.

Major comments "Ma"

1. "*The introduction is incomplete. The authors only provided a review of the previous studies done by themselves and their colleagues, and they neglected the key papers and contributions done by the other researchers who worked extensively on this topic (e.g., Research group at JHU, EPFL, KU-Leuven, . . .).*"

The literature overview was extended and the introduction was completely revised. References about hot-wire measurement to investigate the wake under different operating conditions like yaw misalignment can be found at **R2:Ma1-a** (page 1, line 22). Further information about the measurement of mean velocity and turbulence intensity was integrated at **R2:Ma1-b** (page 2, line 25). References about further applications and benefits of wind tunnels can now be found at **R2:Ma1-c** (page 2, line 31) and references about the investigation of the blockage ratio were now added at **R2:Ma1-d** (page 2, line 43) and **R2:Ma1-e** (page 2, line 49).

2. "*The objective of the work is performing numerical simulations to validate the experimental data. However, the results presented in the paper cannot be considered as a validation. There is a huge discrepancy between the experimental data and numerical results and the authors did not explain the reasons behind that. The authors should perform systematic experimental and numerical experiments with providing a clear explanation of the observed discrepancies. Similar studies have been extensively performed by the other groups which some of them mentioned above. For example, the results presented in Figure 21 cannot be considered as validation. There is a huge difference between the experimental data and simulation results. Besides, the authors mentioned: "The curve for the baseline blade is missing in the current plot as the sensors had a malfunction during the measurement." This statement is not acceptable for a paper that is going to be published in a journal. The same trend is also presented in the other figures. No clear explanations are provided about the differences.*"

We agree with the reviewer's assessment with respect to the measurements of the bending moment but are confident with the on-blade velocity, AoA and flow field measurements.
Strong fluctuations are visible in the raw data of the measured bending moments and heavy filtering was necessary to obtain the distributions shown in the first version of this manuscript. We agree that the resulting data should only be used for qualitative comparison to numerical results but cannot be considered as valid basis for quantitative comparisons and code validation purposes. We therefore decided to discard all measured bending moments in the revised version of the manuscript.
The reason for the removal is given at **R2:Ma2-a** (page 16, line 351). Moreover, the text was adopted and the corresponding passages were removed, see **R2:Ma2-b** (page 1, line 12), **R2:Ma2-c** (page 1, line 13), **R2:Ma2-d** (page 3, line 80), **R2:Ma2-e** (page 29, line 569) and **R2:Ma2-f** (page 33, line 639). The corresponding figures (Fig. 19 and Fig. 20) were adopted, too.
As one of the objectives is the comparison of a medium and a high fidelity code, we consider a comparison of the bending moments calculated with the two numerical methods important. Especially for future simulations including flaps, which will be explained in more detail in the next Major Comment (Ma3).
However, the QBlade results were revised and improved in the course of another Paper (Marten et al. 2018). They were replaced in the present manuscript, too, to provide the latest results.

In this concerning paper, the present manuscript was cited. In the former QBlade simulations, the size of the vortex was estimated too large. Instead of the time offset, the parameter "initial vortex core size" is used now in the vortex evolution equation. This parameter is more common in literature and better defined. In the present investigation, approximately 10% midspan chord are used for this parameter, leading to a 50% smaller vortex core. The relevant parameters for the QBlade simulation are now listed in Table 3.
The authors consider the experimental data for the on-blade velocity and the AoA suited for validation, as the progression of the curves and the differences between simulation and experiment can be explained. Explanations which were already included in the first submission of the manuscript can be found, for example, at **R2:Ma2-h** (page 21, line 450) or **R2:Ma2-i** (page 26, line 521). The differences between the measured and simulated velocity planes are bigger, but can still be explained, see for example **R2:Ma7-b** (page 16, line 373) or **R2:Ma2-j** (page 17, line 380).
More explanations about the differences are now added in the text, see Major Comment Ma4 (e.g. **R2:Ma4-g** (page 20, line 430)) or Ma5 (e.g. **R2:Ma5-g** (page 22, line 464)).
References of the groups proposed by the reviewer, as well as further references were added, see major comment 1 (Ma1).

3. "*The authors mentioned: "As it is currently not possible to include the wind tunnel walls into the LLFVW simulations of QBlade, far-field simulations were conducted." Since the objective of the paper is exploring the blockage effect, it is not clear what the purpose of having the results from the QBlade is. It would be more relevant if the QBlade results considering the wind tunnel wall are added to the paper. Otherwise, it is not needed to add the results from another code that is not consistent with the experimental investigation.*"

The exploration of the blockage effect is only one of the submissions's objectives. Actually, the aims of the present study are threefold, compare the revised abstract (**R2:Ma3-a** (page 1, line 2)) and introduction (**R2:Ma3-b** (page 3, line 64)). One of these aims is the "comparison and evaluation of methods of high fidelity like Computational Fluid Dynamics and medium fidelity like Lifting Line Free Vortex Wake" (**R2:Ma3-c** (page 1, line 5)), respectively "the comparison of codes with different grades of fidelity" (**R2:Ma3-d** (page 3, line 66)). This objective was achieved as it could be shown, that the lack of wind tunnel walls in the QBlade simulation only led to a constant offset regarding on-blade velocity and AoA. This is an important information concerning further investigations with QBlade.
Unfortunately, as mentioned in the manuscript (**R2:Ma3-e** (page 9, line 196)), the consideration of wind tunnel walls in QBlade is not possible, yet. Therefore, no QBlade results including the wind tunnel walls are available so far.
However, one of the advantages of QBlade is the fact, that it can produce results very fast compared to CFD codes. Therefore, it is well suited, for example, for parametric investigations, controller design or load calculations etc.. The investigations presented in this submission are performed in the course of the DFG PAK 780 project. One of the objectives of the project is the investigation of active trailing edge flaps. These flaps are already integrated in the model wind turbine, although they are fixed in their neutral position for the experiments discussed in this manuscript (**R2:Ma3-f** (page 8, line 163)). Subsequent measurements on the model wind turbine including flaps shall be used to validate the implementation of the flaps in the CFD and LLFVW code, so they can be used to build the bridge to full size turbines afterwards.
Though, prior to the investigations including flaps, the simpler case without actuated flaps was investigated and used to determine the differences between experiment and simulation. The results of this investigation are presented in the present submission.
With the knowledge gained by the comparisons, the LLFVW code could be used to deter-

mine the ideal flap deflection to mitigate known disturbances, for example caused by yaw misalignment, see the two references at the beginning of this document (Marten et al. 2018 and Bartholomay et al. 2018). These mutual comparisons are only possible with the knowledge about the influence of the wind tunnel walls on the QBlade results, see **R2:Ma3-g** (page 33, line 618)
Moreover, after the implementation of the flaps in the CFD and LLFVW code has been validated, the codes can be used to investigate full size turbines, where no wind tunnel walls influence the results. In addition to that, with the possibility of QBlade to produce fast results, the code can be used on the one hand for parametric studies to determine the ideal size and position of the flaps as well as the ideal deflection for a previously known disturbance such as yaw misalignment.
To sum up, the results of the comparison of QBlade results to results of a CFD code and to experiments are an important basis for the assessment of the LLFVW code for further investigations of the model wind turbine including flaps.
For these reasons, the authors considered the inclusion of QBlade results relevant as basis for future studies. The authors hope, that these explanations could show the reviewer the importance of the comparisons with QBlade, even as the simulations neglect the effect of the wind tunnel walls.

4. "*As it is mentioned before, the validation section is not acceptable. Also, since Figures 9 and 10 are qualitative results, the authors need to provide more quantitative comparisons by, for instance, comparing the results at different locations. Although, even from the contour plots, the agreement is not good. Also, besides the mean velocity, the variances obtained from both the experiment and numerics should be provided. This is a very standard way for validation of numerical tools against the experimental data.*"

The authors want to apologize for the insufficient validation section. The complete chapter was revised and more qualitative comparisons along with interpretations were added
In the manuscript, the measured and the simulated flow fields are compared at two locations (one upstream and one downstream of the rotor). At another location (+1.05d downstream) further measurements were performed and simulation data for that plane is also available. However, the authors decided to forego the comparison at this location as the evaluation would not have brought further benefit or pursuing information for the submission.
Moreover, at this location, the influence of the nozzle is already present, which influences the wake development further. This is now also mentioned in the text, see **R2:Ma4-a** (page 16, line 364). But the data are available and could be included.
According to reviewer 1 Major Comment Ma3.4 and **R2:Ma7-b** (page 16, line 373), more information about the inequalities in the measured inflow velocity are addressed now. Moreover, according to **R2:Ma7-a** (page 5, line 118), a comment on the turbulent inflow field is added.
To consider the reviewer's request for more quantitative results, the authors included tables with the streamwise mean velocity, the standard deviation of the streamwise velocity as well as the global turbulence intensity in x-y-direction for both locations, see Table 5 **R2:Ma4-b** (page 17, line 383) and Table 6 **R2:Ma4-e** (page 19, line 418). Compare also reviewer 1 Major Comment Ma 3.4.
We prefer to show the standard deviation instead of the variance to be consistent within the whole manuscript, as the standard deviations are now already inserted for different parameters, like the on-blade velocity, see **R2:Ma4-s** (page 21, line 451), **R2:Ma4-t** (page 22, line 476) and **R2:Ma4-u** (page 24, line 493) and the AoA, see **R2:Ma4-h** (page 25, line 512), **R2:Ma4-v** (page 26, line 542) and **R2:Ma4-w** (page 29, line 562). Moreover, the mean differences between measurement and simulation were determined and mentioned in the text, see **R2:Ma4-d** (page 18, line 395) and **R2:Ma4-g** (page 20, line 430).

Moreover, information about the measurement uncertainty is now included in the revised manuscript, see **R2:Ma4-cc** (page 15, line 329) and **R2:Ma4-dd** (page 14, line 297). The authors want to remark, that for the present investigations, which are a basis for the subsequent investigations of the wind turbine including flaps, the focus was not on the detailed reproduction of the unsteady inflow conditions. This will be the content of a future study, were the turbulent parameters from the measurement are used to create unsteady inflow conditions for the CFD simulations. This was also mentioned in the submission now, see **R2:Ma7-f** (page 18, line 392).
Now, quantitative results of the velocity planes are discussed in the text, see **R2:Ma4-c** (page 17, line 385), **R2:Ma4-x** (page 17, line 387), **R2:Ma4-f** (page 19, line 420), **R2:Ma4-z** (page 19, line 423), as well as **R2:Ma4-p** (page 33, line 624) and **R2:Ma4-q** (page 33, line 625). Moreover, quantitative comparisons are added for the other parameters. Concerning the on-blade velocity, see Table 7, 8 and 9, concerning the AoA, Table 10, 11 and 12. The references concerning the discussion of this tables can be found under Major Comment Ma5.
Additionally, the statement concerning the agreement was revised, see **R2:Ma4-bb** (page 21, line 436).
Quantitative comparisons concerning the bending moments as well as explanations can be found at 13 **R2:Ma4-i** (page 29, line 574) and 14 **R2:Ma4-n** (page 32, line 592) as well as on **R2:Ma4-k** (page 29, line 577), **R2:Ma4-l** (page 30, line 579), **R2:Ma4-m** (page 30, line 583), **R2:Ma4-o** (page 32, line 594), **R2:Ma4-j** (page 29, line 575),

5. "*Figure 13-16, it seems that the y-axis chosen here is too wide to minimize the difference between the experiments and numerics. For example, in Fig. 13 (left), it is trivial that the on-blade velocity cannot be ranged from 0 to 30. In particular, considering the tip-speed ratio and the incoming wind speed, it should be in a much narrower range.*"

The authors assume, that the reviewer refers to Fig. 13-15 (now, due to the suggestions of reviewer 1, Mi24 Fig. 12, Fig. 13 and Fig. 14), as Fig. 16 (now Fig. 15) already shows the angle of attack.
The authors totally agree with the reviewer, that the on-blade velocity cannot range from $0m/s$ to $30m/s$. The range of the y-axis in the manuscript reached from $15m/s$ and $30m/s$ and the range of the x-axis from 0° to 360°. Due to the proximity of the labels for x- and y-axis, they can easily be mixed-up at the coordinate origin.
Initially, the range of the y-axis from $15m/s$ to $30m/s$ was chosen primary for reasons of comparability. Now, the y-axis of Fig. 12, Fig. 13 were adopted to be better adjusted to the occurring velocities. However, the axis range at both radial positions were kept the same for all the cases. Thereby, the level difference between $65\%R$ and $85\%R$ becomes more obvious for each case. Therefore, the axis range of Fig. 14 could not be reduced.
For an even better comparison, the authors added tables (Table 7 **R2:Ma5-a** (page 22, line 453), Table 8 **R2:Ma5-h** (page 22, line 477)) and Table 9 **R2:Ma5-l** (page 24, line 494)) where the average of the differences between experiment and the different simulations and evaluation methods are listed. The undisturbed velocity was chosen as reference, so the cases can be compared over the different yaw angles, as all differences have the same reference velocity, see **R2:Ma5-b** (page 22, line 456) and **R2:Ma5-c** (page 22, line 457). Moreover, the contents of the tables are discussed in the text, see **R2:Ma5-d** (page 22, line 458), **R2:Ma5-e** (page 22, line 460), **R2:Ma5-f** (page 22, line 462), **R2:Ma5-g** (page 22, line 464), **R2:Ma5-i** (page 23, line 480), **R2:Ma5-j** (page 23, line 481), **R2:Ma5-k** (page 23, line 482), **R2:Ma5-m** (page 24, line 497).
Through this approach, the comparability of the single figures at the different rotor locations remains, but the assessment of the differences of the single curves is improved.

In order to improve the analysis of the angle of attack, too, tables to assess the quantitative differences between experiment and simulation were added as well at Chapter 4.3 (Table 10 **R2:Ma5-n** (page 25, line 509), Table 11 **R2:Ma5-t** (page 26, line 539) and Table 12 **R2:Ma5-w** (page 28, line 556)). Again, the contents of the tables are discussed in the text, see **R2:Ma5-o** (page 25, line 516), **R2:Ma5-p** (page 26, line 520), **R2:Ma5-q** (page 26, line 523), **R2:Ma5-r** (page 26, line 531), **R2:Ma5-s** (page 26, line 531), **R2:Ma5-u** (page 26, line 541), **R2:Ma5-v** (page 27, line 546), **R2:Ma5-x** (page 28, line 560), **R2:Ma5-y** (page 29, line 562) and **R2:Ma5-z** (page 29, line 564) and additional explanations for the differences are provided, see **R2:Ma5-aa** (page 26, line 523) and **R2:Ma5-bb** (page 27, line 547).
Concerning quantitative comparisons of the bending moments, see the references under Major Comment Ma2.

6. "*Most of the citation about the numerical frameworks are technical report, conference proceeding or personal communications. Typically, it is expected that the papers cited in the manuscript were peer-reviewed before.*"

The authors apologize for the lack of peer-reviewed manuscripts on preparatory work for the present study. Journal publications are underway. As there are lots of investigations and further developments are going on right now and the publication in journals take some time, the authors used the technical reports, and conference proceedings to offer the reader further information, whose detailed provision would have been beyond the scope of the present submission.
The authors are happy to inform the reviewer, that one manuscript was accepted in Wind Energy in the meanwhile and will replace two personal communications (Jost, 2017 and Klein, 2017 –> Jost et al, 2018) in the present manuscript, see **R2:Ma6-a** (page 15, line 339). The corresponding text in the manuscript was adopted according to this fact, see **R2:Ma6-b** (page 15, line 339), **R2:Ma6-c** (page 15, line 343) and **R2:Ma6-d** (page 16, line 346).

7. "*The incoming flow is not characterized in the manuscript. The information about the incoming wind, the associated turbulence level, the Reynolds number based on the chord length is missing in the manuscript.*"

Additional information about the inflow is now added in Subsection 2.2.1 see **R2:Ma7-a** (page 5, line 118) and in Subsection 4.1, see **R2:Ma7-b** (page 16, line 373). Moreover, related to Major Comment Ma4, further information about the velocity fields were added in the text. A threshold for the turbulence intensity in the settling chamber is provided in the text, see **R2:Ma7-c** (page 5, line 117) as well as the mean Ti in the velocity planes (compare Table 5 and Table 6).
As suggested by reviewer 1, the Reynolds number at the blade root was added, see **R2:Ma7-d** (page 6, line 133). Moreover, a representative Reynolds number at 75%R was added in Table 2. This position is located in the middle between the two 3-hole probes, which are used for the determination of the on-blade velocity and the angle of attack.
In future studies, the measured unsteady inflow will be used to create unsteady inflow conditions for the *CFD* simulation. Those planned simulations are now mentioned in the text, see **R2:Ma7-f** (page 18, line 392).
A picture of the measured horizontal velocity is added in this document.

The horizontal velocity shows the upstream effect of the turbine, as the flow bends to the negative direction for y<0 and in positive direction for y>0. As the horizontal velocity is more than one order of magnitude smaller than the axial velocity, it has only a minor effect on the

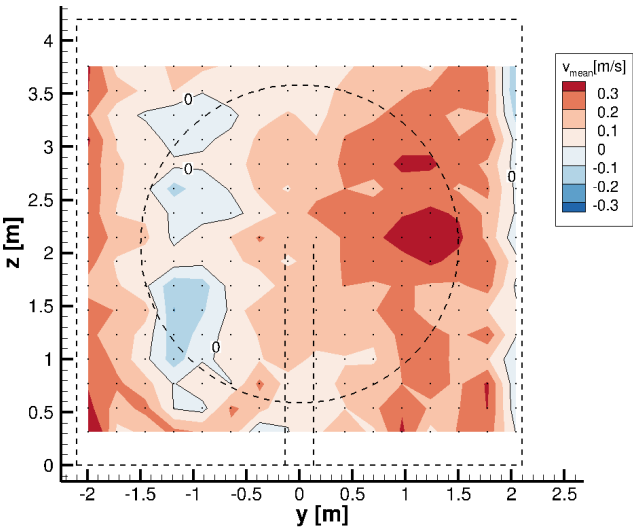

Figure 1: Hot-wire measurements of the y-velocity $0.43d$ upstream of the rotor plane. The dashed lines illustrate the wind tunnel and the turbine. Isolines show a velocity of $0.0ms^{-1}$. The dots show the discrete measuring points.

AoA and on-blade velocity. Consequently, it was not shown in the revised submission in order to keep it concise.

8. "*The results are provided without any sensitivity analysis to the grid resolutions. As mentioned before, the agreement between the numerical results and experiment is poor. Although the code might have tested before for other cases, it is required to perform the grid resolution sensitivity for this particular analysis presented in the manuscript. The convergence of the statistics also should be provided*"

The authors agree, that a sensitivity analysis of the grid resolution is very important for CFD simulations. For this reason, a grid convergence study according to Celik et al. (2008), where the dependency of the numerical solution on the grid resolution was estimated, was performed prior to the present investigation. The results were already published in Fischer et al. (2018) and the reference is mentioned in the present manuscript, see **R2:Ma8-a** (page 12, line 267). The investigation in Fischer et al. (2018) was performed for a one third model of the model wind turbine in a far field environment under uniform inflow. But as the number of cells for the present setup was kept constant or was even increased, for example for the blades, a renewed grid convergence study for the full model was not performed. In order to achieve an easier and better assessment of the sensitivity analysis of the grid resolution for the reader, the authors added further information about the sensitivity analysis from the corresponding paper (Fischer et al., 2018) , see **R2:Ma8-b** (page 12, line 268).
Overall, 45 rotor revolutions were calculated. The results presented in this manuscript are the averaged data over the last five revolutions. The difference between e.g. the global loads of the rotor averaged over revolution 36-40 to the loads averaged over revolution 41-45 amounts 0.03%. This information was partly already included in the first submission. The missing information was now added and can be found at **R2:Ma8-c** (page 13, line 276).

List of the major changes in the manuscript

The line numbers correspond to the marked-up manuscript, not ot the revised version of the manuscript.

- Abstract
  - page 1, line 1-16: completely revised

- 1 Introduction
  - page 1-3, line 18-78: completely revised, literature overview extended

- 2 Methodology and setup
  - page 3, line 86-88: overview of section added
  - page 4, line 89: section 2.1 pulled forward and change of title
  - page 5, line 106-108: overview of section added
  - page 5-6, line 111-127: information about wind tunnel added
  - page 6, Figure 2: caption extended
  - page 6-8, line 132-151: additional information concerning Reynolds number, main goal of the turbine and blockage ratio added
  - page 7, Figure 3: replaced
  - page 8, line 156: titel of subsection changed
  - page 8, line 162-173: section extended
  - page 9, Figure 4, left: position of zz tape added
  - page 9-10, line 200-212: advantage of LLFVW over BEM added
  - page 10, Table 3: extended
  - page 12-13, line 267-271: information about grid convergence added
  - page 13, line 276-277: number of rotor revolutions added

- 3 Data acquisition
  - page 13, line 279: new subsection
  - page 13, line 280-283: overview of section added
  - page 14, line 289-291: information about measurement time added
  - page 14, line 292-296: information about probe calibration added
  - page 14, line 297-301: information about measurement uncertainty added
  - page 15, line 323-324: information about typical corrections added
  - page 15, equation 1 added
  - page 15, line 329-333: information about measurement uncertainty added
  - page 16, line 351-353: information about lack of measured bending moments added

- 4 Results and discussion
  - page 16, line 364-366: information about additional plane added
  - page 16-17, line 374-377: information about velocity plane added
  - page 17, line 380-382: information about inequalities added
  - page 17-18, line 383-392: information about inflow added
  - page 17, Table 5 added
  - page 19, line 410-413: information about influence of turbulence added
  - page 19-20, line 418-427: quantitative comparison extended

- page 20, Table 6 added
- page 20-21, line 429-435: quantitative comparison extended
- page 21, line 444-450: information about inequalities added
- page 21-22, line 450-462: quantitative comparison extended
- page 22, equation 2 added
- page 22, Table 7 added
- page 22, line 464-473: explanations extended
- page 22-23, line 476-485: quantitative comparison extended
- page 23, Table 8 added
- page 24, line 493-495: quantitative comparison extended
- page 24, Table 9 added
- page 24-25, line 498-500: quantitative comparison extended
- page 25, line 509-517: quantitative comparison extended
- page 26, Table 10 added
- page 26, line 521-527: explanations extended
- page 26, line 531-533: quantitative comparison extended
- page 26, line 542-544: quantitative comparison extended
- page 27-28, line 547-552: explanations extended
- page 28, Table 11 added
- page 28, Figure 18, right: name corrected
- page 28-29, line 560-564: quantitative comparison extended
- page 29, Table 12 added
- page 29, line 569-571: overview of section added
- page 29, Table 13 added
- page 30, Figure 19: measured bending moments removed
- page 30-31, line 583-588: quantitative comparison extended
- page 31, Figure 20: measured bending moments removed
- page 32, Table 14 added
- page 32, line 592-603: quantitative comparison extended
- page 32, line 604-607: short summary added

- 5 Summary
  - page 32-34, line 609-659: completely revised

- Achnowledgement
  - page 34, line 670-671: extended

- References
  - page 35-37, line 673-773: several references updated, e.g. Jost et al 2018
  - page 35-37, line 673-773: several new references, e.g. Bastankhah and Porté-Agel 2015

About the suitability of different numerical methods to reproduce model wind turbine measurements in a wind tunnel with high blockage ratio

Annette Claudia Klein[1], Sirko Bartholomay[2], David Marten[2], Thorsten Lutz[1], George Pechlivanoglou[2], Christian Navid Nayeri[2], Christian Oliver Paschereit[2], and Ewald Krämer[1]

[1]University of Stuttgart, Institute of Aerodynamics and Gas Dynamics, Pfaffenwaldring 21, 70569 Stuttgart, Germany
[2]TU Berlin, Chair of Fluid Dynamics, Müller-Breslau-Straße 8,10623 Berlin, Germany

Correspondence to: Annette Claudia Klein (annette.klein@iag.uni-stuttgart.de)

Abstract. **R1:Mi2.1** In the present paper, numerical and experimental investigations of a model wind turbine with a diameter of 3.0m are described. **R1:Mi2.2-a** **R2:Ma3-a** The study has three objectives. **R1:Mi2.2-b** The first one is the provision of validation data. The second one is to **R1:Ma1-b** estimate **R1:Mi2.2-e** the influence of the wind tunnel walls by comparing measurements to simulated results with and without wind tunnel walls. **R1:Mi2.2-d** The last objective is the comparison and evaluation of **R1:Mi2.2-c** **R2:Ma3-c** methods of high fidelity namely Computational Fluid Dynamics and medium fidelity namely Lifting Line Free Vortex Wake. The experiments were carried out in the large wind tunnel of the TU Berlin **Authors** where a blockage ratio of 40% occurs. With the **R1:Mi1-a** Lifting Line Free Vortex Wake code *QBlade*, the turbine was simulated under far field conditions at the TU Berlin. **R1:Mi1-b** Unsteady Reynolds-averaged Navier-Stokes simulations **Authors** of the wind turbine, including wind tunnel walls and under far field conditions, were performed at the University of Stuttgart with the **R1:Mi1-c** Computational Fluid Dynamics code *FLOWer*.
Comparisons between experiment, the **R1:Mi1-e** Lifting Line Free Vortex Wake code and the **R1:Mi1-f** Computational Fluid Dynamics code include on-blade velocity **R1:Ma8-b** **R2:Ma2-b** and angle of attack. Comparisons of flow fields are drawn between experiment and the **R1:Mi1-g** Computational Fluid Dynamic code. **R1:Ma8-c** **R2:Ma2-c** Bending moments are a compared between the simulations.
Authors A good accordance was achieved for the on-blade velocity and the angle of attack, whereas deviations occur for the flow fields and the bending moments.

1 Introduction

R1:Mi8 In order to improve wind turbines, new strategies and concepts have been developed over the last couple of years. Prior to their application on real wind turbines, they have to be analyzed in detail and the underlying processes have to be completely understood. In many cases, investigations take place on model wind turbines, which is less expensive than building a full size prototype. **Authors** Moreover, in wind tunnel tests, reproducible inflow conditions can be created.
R1:Ma1-j **R2:Ma1-a** Bastankhah and Porté-Agel (2015), for example, investigated the interaction between the wake of tur-

bines under yawed conditions. They used particle image velocimetry (*PIV*) for flow physics studies on this complex interaction phenomenon. In subsequent investigations, see Bastankhah and Porté-Agel (2017), they additionally used hot-wire anemometry to analyze the flow upsteam of the turbine, as well as in the near-wake and far-wake regions. **R1:Ma1-f** **R2:Ma1-b** Chamorro and Porté-Agel (2009) used hot-wire anemometry to characterize, amongst others, the distribution of mean velocity and turbulence intensity in the cross section of a wind tunnel at different locations downwind of a wind turbine. Medici and Alfredsson (2006) examined the wake of a model wind turbine under uniform inflow and under the influence of free stream turbulence in terms of 3D effects. For these investigations, as well as for the investigations of a model wind turbine under yaw misalignment, two-component hot-wires were used to measure the velocity fields.

R1:Ma1-g **R2:Ma1-c** Even a micro wind farm can be installed in a wind tunnel to investigate the unsteady loading and power output variability, see Bossuyt et al. (2016, 2017). Howland et al. (2016) used the same experimental setup of the micro wind farm to investigate the power output for a variety of yaw configurations.

R1:Mi9-a Moreover, wind tunnel measurements can be used to validate and further develop numerical codes. In the *MEXICO* project (Schepers and Snel (2007)), comprehensive measurements of a three bladed rotor model of $4.5\mathrm{m}$ diameter have been conducted. The experimental data were used, amongst other, to validate numerical methods. Bechmann et al. (2011), for instance, used the *PIV* data, together with the pressure distribution, to validate their **R1:Mi1-h** Computational Fluid Dynamics **R1:Mi9-b** (*CFD*) simulations. Blind tests, for example of unsteady aerodynamics experiment as done in the NASA-Ames wind tunnel (Simms et al., 2001), can be used to improve the development of wind turbine aerodynamics codes and the provided data can also be used for their validation.

Authors If the model wind turbine is investigated in a closed test section, the wind tunnel walls can influence the results. The extend of this influence depends on the blockage ratio, **R1:Mi34-b** which is defined as the rotor swept area divided by the wind tunnel cross section. **R1:Ma1-h** **R2:Ma1-d** Schreck et al. (2007), as well as Hirai et al. (2008), investigated model wind turbines in wind tunnels with a blockage ratio of approximately 10% and made no blockage correction. Chen and Liou (2011) quantitatively investigated the effects of tunnel blockage on the power coefficient of a horizontal axis wind turbine in a wind tunnel through experiments. They confirmed the results of Schreck et al. (2007) and Hirai et al. (2008), as they found, that the blockage correction is less than 5% for a blockage ratio of 10%. **R1:Mi34-a** Schümann et al. (2013), who experimentally investigated the wakes of wind turbines in a wind tunnel, also showed that for a blockage ratio smaller than 10%, no blockage effect should be experienced and the wind tunnel walls can be neglected. **R1:Ma1-i** **R2:Ma1-e** Sarlak et al. (2016) performed Large Eddy Simulations (*LES*) in order to investigate the blockage effects on the wake and power characteristics of a horizontal-axis wind turbine. Thereby, the turbine was modelled with the actuator line technique. They found, that for the operation of the wind turbine close or above the optimal tip speed ratio, even blockage ratios which are larger than 5% will have a substantial impact on the turbine performance.

Authors Fischer et al. (2018) performed **R1:Mi1-j** unsteady Reynolds-averaged Navier-Stokes (*URANS*) **Authors** simulations of a model wind turbine in a cylindrically shaped wind tunnel. **R1:Mi3-a** To save computational time, the rotational symmetry of the turbine was exploit and only one third of the rotor was simulated. In such a $120°$-model, periodic boundary conditions are used, solely one blade is taken into account and the tower is neglected. **Authors** In this wind tunnel, the

blockage ratio is $> 50\%$. A strong influence of the wind tunnel walls was experienced leading to a more than **R1:Ma1-a** 60% increase of the driving forces and 25% of the thrust in average. The full model of the same turbine in the real wind tunnel (blockage ratio 40%) was simulated by Klein et al. (2018). Thereby, an increase of 25% in thrust and 50% in power was experienced.

R1:Ma1-c But until now, the performance of a model wind turbine at such a high blockage ratio has not been verified with experimental data.

R1:Mi11-a **R2:Ma3-b** Thus, the provision of experimental data for the validation of the numerical approaches is one of the three objectives of the present study. **R1:Ma1-e** The second is the estimation of the influence of the wind tunnel walls. It will be evaluated by comparing *CFD* simulations with and without wind tunnel walls to experimental data. **R1:Mi11-c** **R2:Ma3-d** The third deals with the comparison of codes with different degrees of fidelity.

R1:Mi2.4-a In the present paper, **Authors** the same model wind turbine and wind tunnel as used by Klein et al. (2018) will be investigated experimentally and numerically. **R1:Mi2.4-c** The studied Berlin Research Turbine (*BeRT*), see Pechlivanoglou et al. (2015), was designed and built by TU Berlin and *SMART BLADE GmbH* with a contribution of TU Darmstadt in the aerodynamic blade design. **Authors** The measurements are conducted in a circuit wind tunnel and the simulations are performed with two methods with different degrees of complexity. A Lifting Line Free Vortex Wake **R1:Mi1-i** (*LLFVW*) code (*QBlade*) simulates the turbine under free stream conditions. In the numerical setup of the *CFD* code *FLOWer*, the wind tunnel walls and the nozzle are taken into account, but also a case with far field is simulated in order to **Authors** estimate the influence of the wind tunnel walls and to enable a better comparison to the *QBlade* results.

Authors One baseline case and two different **R1:Mi10** yaw-misalignment cases of the turbine are investigated in this study.

Authors All simulations are conducted with uniform inflow. At cutting planes upstream and downstream of the turbine, velocities are compared between experiment and *FLOWer*. The on-blade velocities and angles of attack (AoA), as seen by defined blade sections, are compared between experiment, *QBlade* and *FLOWer*. As the determination of the AoA in *CFD* is complex, two different methods are used in *CFD*. Moreover, the bending moments at the blade root are compared between **R1:Ma8-d** **R2:Ma2-d** *QBlade* and *FLOWer*.

The numerical and experimental investigation of the turbine is part of the *DFG PAK 780* project (Nayeri et al., 2015), where six partners from five universities work together in the field of wind turbine load control.

2 Methodology and setups

R1:Ma3.1-a In the following, an overview of the characteristics of the setups is given in subsection 2.1. The experimental setup is described in detail in subsection 2.2, followed by the description of the numerical methods and setups of *QBlade* (subsection 2.3) and *FLOWer* (subsection 2.4).

2.1 Overview and general characteristics of the setups

R1:Mi22-a **R1:Ma3-a** **R1:Ma3.1-b** As the paper deals with a multitude of cases and setups, the following subsection gives an overview and summarizes the particular characteristics of the setups.

As, according to Schepers (2012), wind turbines are exposed to yaw misalignment from 2% up to 10% of their operating time, these load cases play an important role in wind energy. Therefore, three different cases concerning the inflow direction are taken into account in the present paper. $CaseBASE$ corresponds to the turbine **Authors** with no yaw misalignment. In $CaseYAW15$, the turbine is rotated by $-15°$ **R1:Mi4** (clockwise) around the vertical axis of the rotor plane. Usually, a turbine is rotated around the tower. However, as the model wind turbine is placed in a wind tunnel, a rotation around the tower would lead to different clearance distances of the blades to the wall for one revolution. Therefore, the turbine is rotated around the z-axis of the rotor in order to achieve a constant distance between blade tip and wind tunnel walls over a whole revolution. $CaseYAW30$ is rotated by $-30°$. **Authors** In all simulations uniform inflow is considered. The experimental results have the affix $_{Exp}$, the ones of *QBlade* $_{QBlade}$ and the *FLOWer* results are designated by $_{FLOWer}$. The far field case of *FLOWer* has the addition $_{-FF}$. Table 1 gives an overview of the different cases.

Fig. 1 shows the surfaces of $CaseBASE_{FLOWer}$ and $CaseYAW30_{FLOWer}$. There, the unusual position of the nozzle,

Table 1. Overview of the cases.

Wind tunnel			
Yaw	Experiment	*QBlade*	*FLOWer*
$0°$	$CaseBASE_{Exp}$	—	$CaseBASE_{FLOWer}$
$-15°$	$CaseYAW15_{Exp}$	—	$CaseYAW15_{FLOWer}$
$-30°$	$CaseYAW30_{Exp}$	—	$CaseYAW30_{FLOWer}$
Far field			
Yaw	Experiment	*QBlade*	*FLOWer*
$0°$	—	$CaseBASE_{QBlade}$	$CaseBASE_{FLOWer-FF}$
$-15°$	—	$CaseYAW15_{QBlade}$	—
$-30°$	—	$CaseYAW30_{QBlade}$	—

R1:Mi22-b which will be explained in section 2.2.1, and the uncommon yaw movement become obvious.

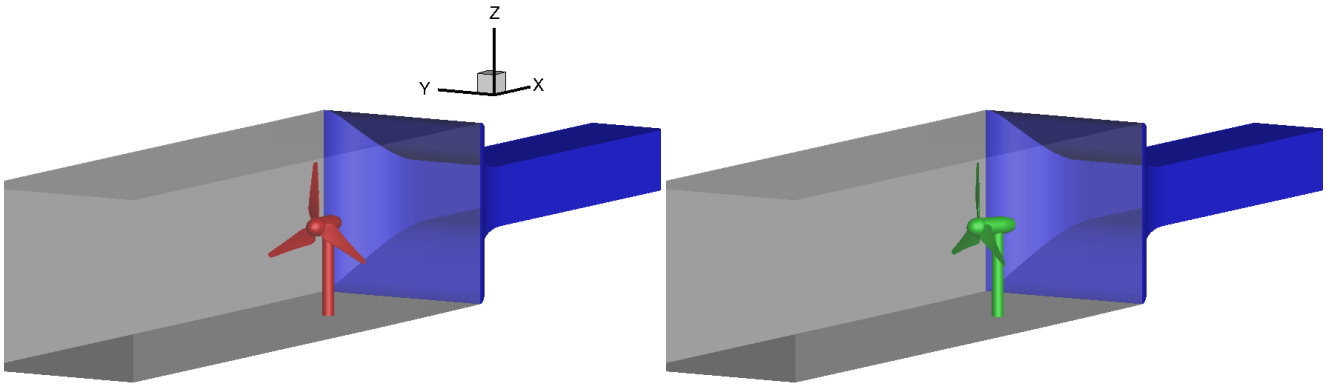

Figure 1. Surface for $CaseBASE_{FLOWer}$ (left) and $CaseYAW30_{FLOWer}$ (right).

2.2 Experimental setup

R1:Ma3.1-c The experimental setup consists of the wind tunnel and the model wind turbine, which will be described in the following sections. The blades of the model wind turbine are described in detail in an additional section, as they deliver the data for the comparison with the numerical solutions.

2.2.1 Wind tunnel

The experiments are carried out in the large wind tunnel (*GroWiKa*) of the TU Berlin, Fig. 2 (Bartholomay et al., 2017), **R1:Ma3.2-a** which is a circuit wind tunnel **R1:Ma3.3-a** and is driven by a $450\mathrm{kW}$ fan. **R1:Ma3.4-a** The $2 \times 1.4\mathrm{m}^2$ cross section of the real test section is too small for the model wind turbine, which has a large diameter to realize the investigation of spanwise locally distributed devices for passive and active flow control in future investigations. Therefore, the real test section was shortened and the $4.2 \times 4.2\mathrm{m}^2$ settling chamber of the wind tunnel was extended to a total length of $5\mathrm{m}$ and was then used as measuring section for the model wind turbine. **R1:Ma3.2-b** This configuration leads to the unusual fact that the nozzle is positioned downstream of the measuring section. **R1:Ma3.3-b** The velocity in the settling chamber used for the present investigations amounts **R1:Mi7-a** $6.5\mathrm{ms}^{-1}$ and the **R2:Ma7-c** turbulence intensity is in average $Ti \leq 1.5\%$ **R1:Ma3.4-b** **R2:Ma7-a** and shows a fairly homogeneous distribution. Three screens are placed upstream of the turbine which aim at increasing the homogeneity in the flow. Additionally, one filtermat is installed at the position of the most upstream screen. Nonetheless, the turbulence intensity is higher in the settling chamber compared to the original test section and the inflow velocity is not perfectly homogeneous. More information about the x-velocity can be found in subsection 4.1 or in Bartholomay et al. (2017). **R1:Ma3.4-d** The turbulence in the inflow might lead to a faster recovery of the wake and to higher fluctuations of the loads compared to a case with lower turbulence. As the wind tunnel is short, the influence of the turbulence on the vortex breakdown might be less pronounced than in a far field case or in a longer wind tunnel. Moreover, Medici and Alfredsson (2006) showed, that up to $x/d = 2$, the initial wakes for a case with and without free stream turbulence are quite similar, even with a higher turbulence intensity as in the present setup. However, the blockage ratio by Medici and Alfredsson

(2006) was less than 3% and consequently much smaller than in the present case.

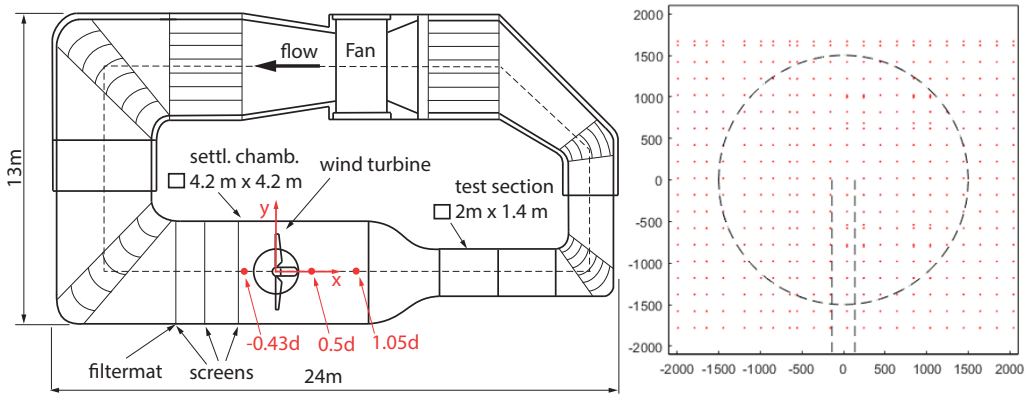

Figure 2. Large wind tunnel of the TU Berlin (left) and hot-wire measurement position in each cross-plane (right), (Bartholomay et al., 2017). The dashed lines in the right picture indicate the rotor and the tower.

2.2.2 Berlin Research Turbine (*BeRT*)

The Berlin Research Turbine (*BeRT*), Fig. 3, has a rotor diameter of 3m with a tower height of 2.1m. The three blades are exchangeable and equipped with the *Clark-Y* airfoil throughout the complete blade radius from tip to hub. This airfoil **R1:Mi12-a** has a maximal thickness of 11.8% and was used as it provides attached flow for **R1:Mi12-b** low Reynolds numbers, as they occur in the blade root region **R1:Mi12-c** **R2:Ma7-d** (e.g. $Re_{15\%R} = 170000$). **Authors** Moreover, it has a good effectiveness of flaps, which will be investigated on the turbine in future experiments and simulations. The twist was chosen so that the local angle of attack stays constant over the span. In order to get a defined transition position for the *CFD* simulations, zig-zag tape has been placed on the blades. The height of the turbulator **R1:Mi13** was estimated experimentally in an additional 2D experiment. It is adapted to the Reynolds number, which varies with the rotor radius, and is consequently staggered. It amounts h=0.75mm inboard up to h=0.21mm outboard on the suction side and h=0.95mm inboard up to h=0.50mm outboard on the pressure side. On the suction side, the leading edge of the tape was positioned at 5% chord, on the pressure side at 10% chord. **R1:Mi12-d** As the main goal of the turbine is to deliver data for the comparison to simulations and to test and analyze flow control devices and not to compare the overall performance to a turbine in the free field, a realistic scaling was of subordinate interest.

The turbine data is summarized in Table 2 (Bartholomay et al., 2017; Pechlivanoglou et al., 2015; Vey et al., 2015).

R1:Mi14 The model creates a significant level of blockage of $\beta = A_{BeRT}/A_{tunnel} = 40\%$. This value is far beyond blockage ratios where correction methods have proven their applicability. But as one of the aims of the present study is the comparison between experiment and simulation, and not to quantify the overall performance to a turbine in the far field, the high

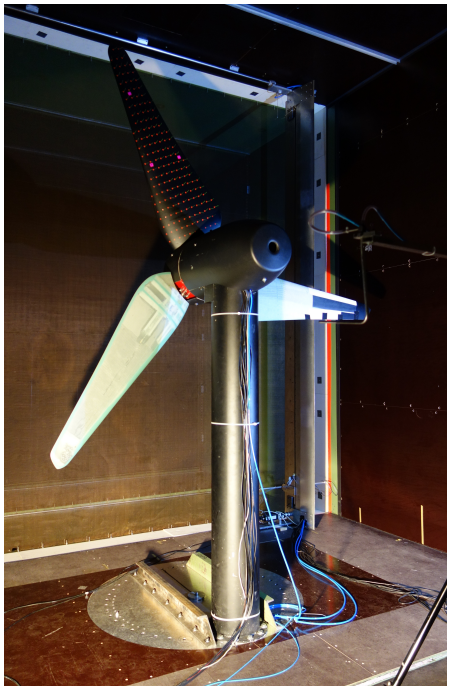

Figure 3. The model wind turbine *BeRT* in the wind tunnel.

Table 2. Summary of the turbine specifics.

Tower height	2.1m
Tower diameter	0.273m
Rotor diameter	3.0m
Rotor overhang	0.5m
Rotor blade airfoil	Clark-Y
Rated RPM	$180 min^{-1}$
Inflow velocity	6.5ms^{-1}
TSR	4.35
3-hole probe position	$65\%R$, $75\%R$, $85\%R$
Reynolds number ($75\%R$)	265000

blockage has only a small impact on the validity of the results.

Data acquisition is achieved by *National Instrument* hardware in the rotating and in the non-rotating system. In the former, a

R1:Ma3.6-a *cRIO* 9068 platform with 9220 modules rotates with the turbine and acquires data from sensors placed on the blades. In the non-rotating setup, a *National Instruments* **R1:Ma3.6-b** *cDAQ* 9188 with 9220 modules platform collects data from additional sensors, such as tower / nacelle acceleration and tower base strain for thrust measurements. Data transmission between the two systems and the control computer is achieved by *WiFi* connection. Further information on the setup is found in (Vey et al., 2015).

2.2.3 Blades

The turbine is equipped with two baseline blades and one smart blade. The smart blade is equipped with a multitude of sensors and actuators for trailing edge **R1:Mi15** flap deployment, whereas one of the baseline blades is equipped with blade root bending sensors. Besides that, no other sensors or actuators are mounted on the baseline blades (Bartholomay et al., 2017).
The smart blade, Fig. 4, is equipped with pressure ports, strain gauges at the blade root, acceleration sensors at the tip, 3-hole probes to measure the angle of attack at $65\%R$, $75\%R$ and $85\%R$, trailing edge flap actuators and encoders to measure the flap position. **R1:Ma3.6-c** The pressure sensors are *Sensortechnics HCL0075E* and the blade strain gauges are of type *FAE1-A6194-N-35-S6/EL.* **R2:Ma3-f** For the current study, the flaps were not deflected but fixed in their neutral position (Bartholomay et al., 2017). **R1:Ma4-a** The three-hole probes, their holder and tubing change the flow around the blade. The equipment is positioned on the pressure side, as in contrast to the suction side, this side is less prone to separation. It is assumed that the presence of the installation leads to higher camber and therefore a higher local lift. Nonetheless, the installation of multi-hole probes is a common practice on research turbines, see Castaignet et al. (2014); Gallant and Johnson (2016); Pedersen et al. (2017). **R1:Mi26** The strain-gauges for the determination of the blade root bending moments are glued on the bolt, Fig. 4, that connects the blades to the hub. The full-bridge aims to mitigate cross-talk effects that influence the measurement results. Nonetheless, as positioning the strain gauges on the circular bolt is challenging, cross-talk effects are present on the results of the sensors. The main sources of cross-talk are edgewise bending moments on the flapwise sensor and vice versa, axial forces due to weight and centrifugal acceleration, but they can also be caused by the blade twist. The first two effects can be quantified by calibration and compensated for measurements.

2.3 The Lifting Line Free Vortex Wake Code *QBlade*

R1:Ma3.1-d The next two parts describe the numerical methods of *QBlade* and give some information about the numerical setup.

2.3.1 Numerical methods of *QBlade*

The Lifting Line Free Vortex Wake (*LLFVW*) computations in this study are performed with the wind turbine design and simulation tool *QBlade* (Marten et al., 2010, 2016, 2015), **Authors** which is developed at the Technical University of Berlin.

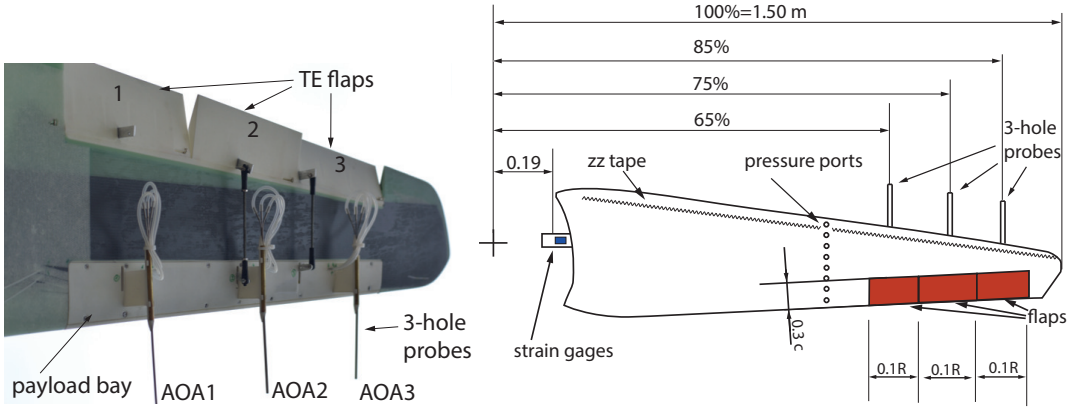

Figure 4. Smart blade, modified from (Bartholomay et al., 2017).

The *LLFVW* algorithm is loosely based on the non-linear lifting line formulation as described by Van Garrel (2003) and its implementation in *QBlade* is used to simulate both HAWT and VAWT rotors.

Rotor forces are evaluated on a blade element basis from tabulated lift and drag polar data. The **Authors** wake is modelled with vortex line elements, which are shed at the blades trailing edge during every time step and then undergo free convection behind the rotor. Vortex elements are de-singularized using a cut off method, as described by Marten et al. (2016), based on the vortex core size. Viscous diffusion in the wake is accounted for through vortex core growths term.

The tower shadow is taken into account by using a model derived from the work of Bak et al. (2001), in which the tower is modelled through a combination of the analytical potential flow around a cylinder superimposed with an empirical downwind wake model based on a tower drag coefficient.

The effects of unsteady aerodynamics and dynamic stall are introduced via the *ATEFlap* aerodynamic model. **Authors** This model reconstructs lift and drag hysteresis curves from a decomposition of the lift polars and has been adapted to be implemented into the free vortex wake formulation of *QBlade*, see Wendler et al. (2016). The computational efficiency of the *LLFVW* calculations is increased through a GPU parallelization of the wake convection step via the OpenCL framework.

2.3.2 Numerical setup of *QBlade*

R2:Ma3-e As it is currently not possible to include the wind tunnel walls into the *LLFVW* simulations of *QBlade*, far field simulations were conducted.

The lift and drag polar data for the rotor's *Clark-Y* airfoil is obtained through *XFOIL* (Drela and GILES, 1987) calculations ($NCrit = 9$ and forced transition at leading edge) for a range of Reynolds numbers and then extrapolated to 360° angles of attack using the Montgomerie method (Montgomerie, 2004). **R1:G4** Although there are similarities between the Lifting Line Free Vortex Wake method and the Blade Element Momentum Theory (*BEM*), the *LLFVW* has a main advantage when compared to *BEM* codes. This advantage comes from the calculation of the induction from the three dimensional representation of

the wake. In this representation the calculation of induction is not limited to an annular averaged rotor disc, but can be accurately calculated at any point in the computational domain and any point in time. In addition to that, the wake always contains the history of the flow (through vortex elements from previous time steps) which gives the ability to simulate transient events with a much higher accuracy than the *BEM*. Furthermore, other induction related effects such as blade hub and tip losses are directly modelled in this formulation. Effects such as yaw error, wake memory, transient or sheared inflow are directly included in the *LLFVW* through the explicit calculation of the wake evolution in three dimensions. Overall the *LLFVW* method relies on far less semi-empirical corrections than the *BEM* when the operating conditions deviate from idealized uniform steady state inflow conditions. And thus it produces results with increased accuracy for a range of operating conditions. The advantages of vortex codes over traditional *BEM* methods, especially in unsteady operating conditions, have already been presented in numerous publications such as Marten et al. (2016); Saverin et al. (2016a, b).

The main simulation parameters used in the *LLFVW* simulation of this study are given in Table 3.

The azimuthal discretization of 5° was chosen to achieve a compromise between computational efficiency and accuracy. The

Table 3. Main parameters of the *QBlade* simulations.

Azimuthal discretization	5°
Blade discretization	21 (sinusoidal spacing)
Maximum wake length	$8rev$
Simulation length	$16rev$
Initial vortex core size	0.025m
Turbulent vortex viscosity	50

wake was fully resolved for eight revolutions to obtain high quality results in rotor plane region, after which it was truncated. **R1:Mi16** This means, that a wake element is removed from the domain after the rotor completes eight full revolutions after it has been released from the blades trailing edge. The blade was discretized into 21 panels in radial direction using sinusoidal spacing to obtain a higher resolution in the tip and hub regions where the largest gradients in circulation are expected. The simulation was carried out over 16 revolutions resulting in 1152 time steps and a maximum of $52,000$ wake segments. Fig. 5 shows a snapshot of the *LLFVW* simulation after four rotor revolutions.

2.4 The CFD Code *FLOWer*

R1:Ma3.1-e In the following, general information about *FLOWer* are given. Moreover, information about the numerical FLOWer setup are provided.

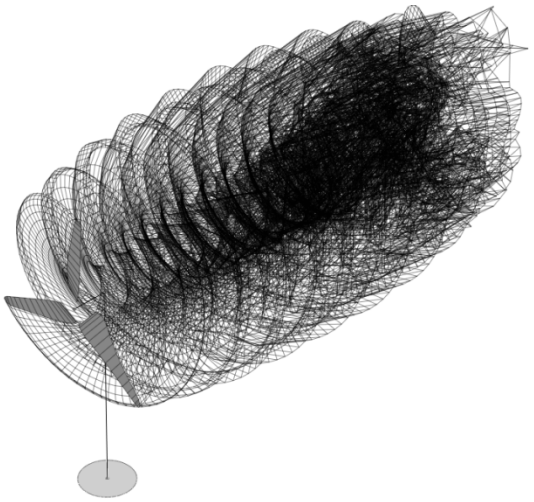

Figure 5. Snapshot of the *LLFVW* simulation after four rotor revolutions.

2.4.1 Numerical methods of *FLOWer*

The *URANS* simulations are carried out using the block-structured solver *FLOWer*, which uses the finite volume method. It solves the compressible Navier-Stokes-Equations and was developed by the German Aerospace Center (*DLR*) in the course of the *MEGAFLOW* project (Kroll et al., 2000) whereas wind energy specific extensions were made at the Institute of Aerodynamics and Gas Dynamics (*IAG*) of the University of Stuttgart. For the temporal discretization, an implicit dual time stepping scheme is used (Jameson, 1991). The space is discretized with a second order central discretization scheme *JST* (Jameson et al., 1981). For the modelling of the turbulence, the Menter *SST* turbulence model is used and the simulations are performed fully turbulent. All components of the setup are meshed separately with a fully resolved boundary layer ($y^+ \approx 1$) and **R1:Mi18** all grids are overlapped, using the *CHIMERA* technique (Benek et al., 1986). The process chain, as used for the present investigations, was developed at the *IAG* (Meister, 2015).

2.4.2 Numerical setup of *FLOWer*

R1:Mi19 The numerical setup consists of eleven grids: background grid (wind tunnel WT or far field FF), hub, nacelle, 3×connection for the blade (blade con), 3×blade, tower and connection for the tower (tower con). The number of cells per grid for all cases can be found in Table 4.

Altogether, the setup in the wind tunnel has 40.1 mio cells. **R1:Mi6** In the far field case, where the wind tunnel walls are not modelled and the background grid has a large expansion, the setup features 38.0 mio cells.

The blade is meshed automatically and is of CH-topology. The boundary layer is fully resolved with 37 grid layers, ensuring $y^+ < 1$ for the first grid layer. Around the airfoil 181 cells were used, in spanwise direction 145 cells for the wind tunnel case and 101 for the far field case. For the wind tunnel case, at around 60% of the radius and at around 90% of the radius, spanwise

Table 4. Cell number in mio of the individual grids for the wind tunnel and far field cases.

Wind tunnel (WT)							
Name	WT	Hub	Nacelle	Blade con	Blade	Tower con	Tower
No. of cells [mio]	11.7	2.2	1.3	0.5	7.2	0.2	1.6
Far field (FF)							
Name	FF	Hub	Nacelle	Blade con	Blade	Tower con	Tower
No. of cells [mio]	14.7	2.2	1.3	0.5	5.5	0.2	1.6

refinements were introduced, which ensure a proper transition for future trailing edge flap deflection. The meshes for all other components, except the far field mesh, are created manually.

Klein et al. (2018) already showed that the wind tunnel walls, the tower and the nozzle behind the turbine have a significant influence on the turbine performance. Therefore, they are taken into account for the present *CFD* simulations. The $4.2 \times 4.2\mathrm{m}^2$ settling chamber **R1:Mi21** of the *GroWiKa* begins $1.245\mathrm{m}$ upstream of the rotor plane and is $5.0\mathrm{m}$ long. As the original test section of the wind tunnel is located behind the settling chamber, in this configuration, the nozzle is located behind the "new" test section. It has a total length of $3.0\mathrm{m}$ and a tapering of 2.2. The wind tunnel walls are realized as slip walls, whereby an approximated displacement thickness, based on the turbulent flow over a flat plate, is added on the real walls. This leads to a constant reduction of the cross section over the whole settling chamber.

In order to prevent the convection of disturbances from the inflow and outflow planes of the computational domain into the measuring section, the wind tunnel was extended to a length of approximately $16.5R$, whereas the rotor plane is located after approximately $7.5R$. The cells around the turbine have an extension of $0.025 \times 0.025 \times 0.025\mathrm{m}^3$. In the direction of the inflow, the cells are stretched up to $0.4\mathrm{m}$ in x-direction, at the outflow, they measure $0.2 \times 0.025 \times 0.025\mathrm{m}^3$. The inflow boundary is realized as far field and at the outflow, a constant pressure is defined in order to maintain mass continuity.

As the wind tunnel and the nozzle could not be taken into account in *QBlade*, yet, a far field case was created, too. Thereby, the refinement for the flaps in the blade mesh was not realized. The background mesh for the far field case was created by an automated script (Kowarsch et al., 2016), which uses hanging grid nodes for the refinement. Usually, in a H-topology, the refinement is not only at the designated spot, but has to be taken along to unnecessary areas. With hanging grid nodes, refinements can be realized only where they are needed. The grid has an overall length of $20.5R$ ($8R$ upstream and $12.5R$ downstream of the rotor), a width of approximately $24.6R$ and a height of approximately $14R$. Consequently, the boundaries are, according to Sayed et al. (2015), far away enough to prevent disturbances on the solution. The boundaries, except the bottom, which is realized as slip-wall, are realized as far field boundary condition. Around the turbine, the cells have a dimension of $0.025 \times 0.025 \times 0.025\mathrm{m}^3$, at the borders $0.1 \times 0.1 \times 0.1\mathrm{m}^3$.

R2:Ma8-a For a one third model a grid convergence index study according to Celik et al. (2008) was already performed (Fischer et al., 2018). **R2:Ma8-b** The extrapolated relative errors between the appropriate grids and the extrapolated values

of a theoretical ideal mesh, which were determined in the course of this investigation, amount 0.63% for power and 0.02% for thrust. As the grids used for the present investigation are partly finer resolved than the ones used in the sensitivity analysis, a renewed investigation for the full model was not performed. **R1:Ma4-b** As the cell number is limited in the numerical simulation and the modelling effort is significant, measuring equipment in the wind tunnel and on the blades was not taken into account.

For the wind tunnel cases, the simulations were performed until convergence of the loads was achieved. This occurs when the difference between the average of torque and thrust over five revolutions and the average of the following five revolutions is $< 0.1\%$. Afterwards, the average of the last five revolutions were used for the evaluation. **R2:Ma8-c** For the present investigation, 45 rotor revolutions were calculated in total. The temporal discretization corresponds to $1.5°$ azimuth and 100 inner iterations for the cases including wind tunnel walls and $1.5°$ azimuth with 30 inner iterations for the far field case.

3 Data acquisition

R1:G1 **R1:Ma3.1-f** This section deals with the data acquisition of the velocity planes, the on-blade velocity and angle of attack as well as of the bending moments for each the experiment and the simulations. **R1:Ma3-b** Fig. 6 shows the position of the velocity planes as well as the evaluation surfaces for the *CircAve* (*LineAve* with circles) method for the AoA determination in *FLOWer* (see subsection 3.2) exemplary at blade 1 and the surfaces used for the *RAV* method of the AoA determination in *FLOWer* (see subsection 3.2).

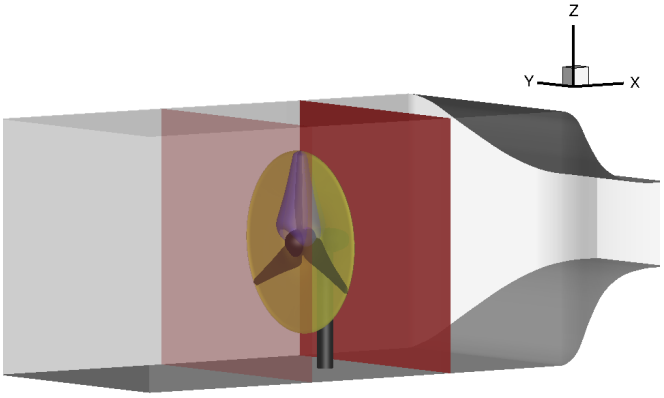

Figure 6. Position of the velocities planes for the *RAV* method (yellow), surface for the determination of the AoA with the *CircAve* method (blue) and velocity planes (red).

3.1 Generation of the velocity planes

R1:Ma3.5 In the experiment, the three red dots in Fig. 2 (left) at **R1:Mi7-b** $x = -0.43d$, $x = 0.5d$ and $x = 1.05d$ indicate where hot-wire measurements are conducted. A semi-automatic traverse with four cross-wire probes with a measurement fre-

quency of $f_s = 25\text{kHz}$ and a cut-off frequency of $f_{cut} = 10\text{kHz}$ is used. Each of the 608 measurement positions, Fig. 2 (right), in each cross-section is measured for $T_s = 16\text{s}$. **R1:Ma5** This time is assumed to be long enough for good statistics for the current setting as the measured integral length scale is $\leq 0.15m$. With the inflow velocity of 6.5ms^{-1} as convective velocity, an integral time of $t = 0.15\text{m}/6.5\text{ms}^{-1} = 0.023\text{s}$ is achieved, which is considerably smaller than the acquisition time of 16s. Offset correction between the probes was realized by repeating **R1:Mi23** 19 measurement points along a vertical line with all four probes. For each measurement position, the mean value of all four measurements was calculated and used as reference. Subsequently, the offset of each probe was calculated. This offset was averaged over all measurement points. Thereby, the offset for each probe was calculated, which was then applied to all measurements in the post-processing. The calibration of the probes was done with the help of a nearby pitot-probe at different wind tunnel velocities.

R1:Ma2-b **R2:Ma4-dd** The error of the hot-wire measurements is the sum of the calibration setup error (pitot-tube, pressure sensor) and the hot-wire anemometry hardware. The latter was calculated by measuring multiple points in each test case with all probes and the largest deviation is defined as the error. In the present case it amounts 3.3%, which corresponds to 0.33ms^{-1} in reference to the maximum calibrated velocity. This is in good agreement with error estimations given in literature, see Finn (2002). The total error, including calibration setup, is calculated to 4.4%, corresponding to 0.44ms^{-1}.

R1:Mi30-a Only the simulation including wind tunnel walls was take into account for the comparison of the velocity planes. In this setup, at each point of the numerical grid, data was extracted for the planes and averaged over five revolutions. In order to evaluate the differences between measurement and simulation, the results of the simulation are interpolated to a grid with the same grid points as the measurement points and the results are subtracted.

3.2 Extraction of the on-blade velocity and the angle of attack

The angle of attack (AoA) is the angle between the velocity, as seen by the blade (on-blade velocity), and the airfoil chord. Generally, deriving an angle of attack in rotating domain is somewhat difficult, as the AoA is a two-dimensional value. Moreover, the blade deflects the streamtraces due to its induction and therefore changes the value of the AoA.

In the experiment the AoA and the on-blade velocity are measured by three-hole probes located at $65\%R$ and $85\%R$. The derivation of the section-wise values, referenced to the quarter-chord point of each section, is detailed by Bartholomay et al. (2017) and will be explained here shortly. Generally, this measurement method is advantageous, as no static tunnel reference pressure is needed and short tubing, as the pressure sensors are located in the blade, mitigates possible delay effects. The three-hole probes measure the α_{probe} and $U_{rel,probe}$ in reference to the probe position upstream of the wing. These values are derived by calibration of the pressure differences between tubes to the flow angle and velocity. However, when mounted on the wing, the results are affected by the induction of the blade and therefore need to be translated into the sectional angle of attack α and the relative velocity U_{rel}. In this project a procedure based on two dimensional flow assumption on the wing, Fig. 7, was employed.

Herein, α_{probe} is first rotated into the local coordinate system, which is based on the local chord, to derive $\alpha_{probe,section}$. Subsequently, a look-up table is used, that was derived by viscous *XFOIL* (Drela and Youngren, 2008) calculations. This table

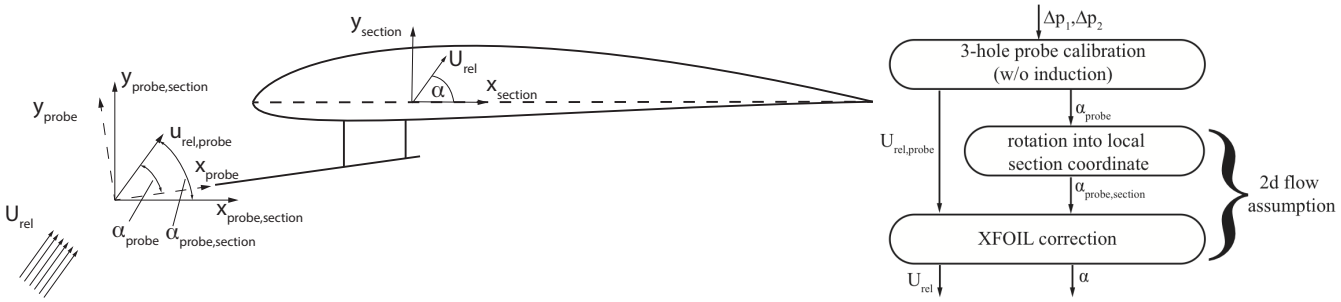

Figure 7. Schematic and flow chart of derivation of the section-wise AoA (Bartholomay et al., 2017).

correlates the measurement at the probes head upstream of the wing to the actual local section angle of attack α. Thereby, the induction effect is accounted for and α and U_{rel} are found. **R1:Mi25** The conversion of the local flow angle at the probe to the actual AoA is almost linear in the linear regime. The approximated equation (Eq. 1) gives information about the order of conversion for this 2D approach.

$$\alpha = 0.58 \cdot \alpha_{probe} - 0.64 \tag{1}$$

The data-set was created by analyzing polars from $\alpha = -30°$ to $30°$ in steps of $0.5°$. Steps in-between are interpolated. This procedure requires two-dimensional flow over the blade, which is assumed to be appropriate in this case, in comparison to quantitative tuft flow analysis (Vey et al., 2015), which indicated little three-dimensional effects on the surface flow.

R1:Ma2-a **R2:Ma4-cc** In order to estimate the measurement error of the three-hole probes, data sets from calibrations of the probe alone and of measurements of the probe installed in a 2D-wing setup were analyzed. The data sets include variation of AoA from $-30°$ to $30°$ and the variation of the free stream velocity. From this analysis, which also includes the error of the induction correction and sensor uncertainties, the maximal absolute error for AoA was estimated to be $0.8°$ (considering only the attached flow regime) and for the on-blade velocity to be $0.4\mathrm{ms}^{-1}$.

In *QBlade*, the angles of attack are evaluated at the quarter chord position of the airfoils at the lifting line (the bound vorticity) of the rotor blades. The angle of attack is calculated from the part of the absolute velocity vector that lies inside the respective airfoils cross sectional plane – which corresponds to the on-blade velocity. The absolute velocity vector itself is a superposition of the inflow, relative, wake-induced and self-induced velocity vectors.

Different methods to derive the effective sectional AoA from 3D *CFD* predicted flow fields are compared and evaluated by **R2:Ma6-a** Jost et al. (2018). Details of the methods **R2:Ma6-b** are described in that manuscript. The two methods, which are most suitable for the present case, are used for the AoA extraction shown in this paper. The reduced axial velocity method (herein after called *RAV*) uses two planes, one upstream and one downstream of the rotor (see Fig. 6). In these planes, the average velocities are calculated and afterwards the velocity components are used to determine the velocity in the rotor plane without the induction of the blade. The method **R2:Ma6-c** bases on the method of Johansen and Sørensen (2004), who determined airfoil characteristics from 3D *CFD* rotor computations. It was successfully applied by Jost et al. (2016) to investigate unsteady 3D effects on trailing edge flaps, and by Klein et al. (2014) for *CFD* analysis of a 2-bladed multi-megawatt turbine. In

the line averaging method (*LineAve* or *CircAve*), **R2:Ma6-d** the AoA is determined by averaging the velocity over a closed line around each blade cut (see Fig. 6). For both approaches, the results are averaged over five revolutions.

3.3 Determination of the bending moments

In the present paper, the flapwise (out-of plane) moment (M_y) and the edgewise (in plane) moment (M_x) are investigated. **R1:Ma8-a** **R2:Ma2-a** Due to problems with the full-bridge strain-gauge setup in the experiment, strong fluctuations are visible in the raw data and heavy filtering was necessary. Therefore, the bending moments can not yet be considered as valid basis for quantitative comparisons and code validation purposes.

In the *LLFVW* method of *QBlade* the blade bending moments are evaluated by summing up the elemental blade forces, obtained from an integration of the normal and tangential forces along the blade span that are obtained via the stored airfoil coefficients.

In the *CFD* simulation, the bending moments in the blade root result from the pressure and friction on the blade surface. For each surface cell the forces are computed and multiplied with the corresponding radius. Then, they are averaged over five revolutions.

4 Results and discussion

4.1 Comparison of the velocity planes

The velocity planes, which are taken into account in the present study, are placed $0.43d$ upstream and $0.5d$ downstream of the rotor plane (see Fig. 6). **R1:Mi27** **R2:Ma4-a** The plane $1.05d$ downstream of the rotor plane (see Fig. 2), is neglected in the present study, as the evaluation would not have brought further benefit for the paper. Moreover, at this location, the influence of the nozzle is already present, which influences the wake development on top of the wind tunnel walls.

Fig. 8 (left) shows the velocity in x-direction for the measurement and the right picture for the *FLOWer* wind tunnel simulation $0.43d$ upstream of the rotor plane. The measuring points are shown as black dots. The dimensions of the wind tunnel, as well as the model wind turbine, are illustrated by dashed lines. Moreover, an isoline with the undisturbed inflow velocity of $6.5\mathrm{ms}^{-1}$ is shown. **Authors** The view direction in this picture, and in all following figures of the velocity planes, is from downstream to upstream.

The turbine blockage effect can be observed in both figures. However, the velocity distribution in the simulation is smoother and axisymmetric, leading to a clearly defined blockage, whereas it is more frayed in the experiment. **R1:Ma3.4-c** **R2:Ma7-b** Due to the location of the settling chamber after a corner, see Fig. 2, the measured x-velocity on the left side differs slightly to the velocity on the right side. Additionally, a difference at the bottom and upper position is apparent. As due to constructive reasons, the mounting of the aforementioned filtermat (see subsection 2.2.1) leaves a small gap at the ceiling of the wind tunnel,

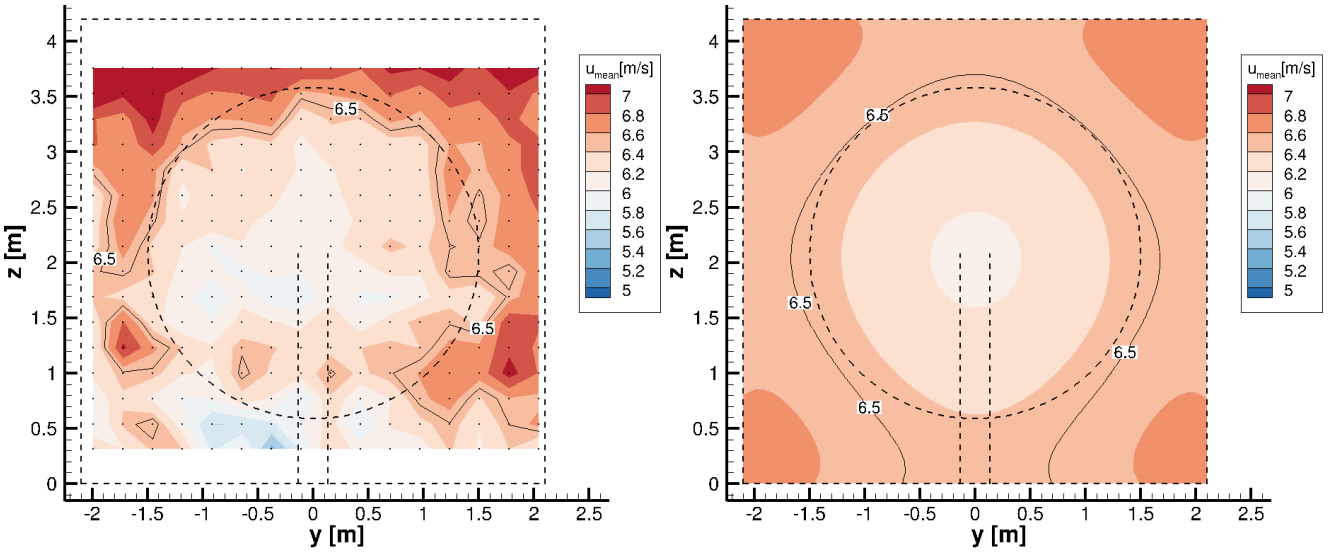

Figure 8. : Hot-wire measurements (left) and simulated velocity plane (right) of the x-velocity $0.43d$ upstream of the rotor plane. The dashed lines illustrate the wind tunnel and the turbine. Isolines show the undisturbed inflow velocity of $6.5\mathrm{ms}^{-1}$. The dots in the left figure show the discrete measuring points.

a small velocity overshoot is present at the top of the inflow test-section. In the simulation, a slightly higher velocity can be seen in the corners of the wind tunnel.

In the experiment, multiple causes of possible measurement errors, such as temperature compensation or induction of the traversing system are analyzed and ruled out. **R2:Ma2-j** Therefore, the horizontal inequalities seem to result from the design of the wind tunnel. More information about **R1:Mi28** the hot wirer measurements and possible reasons for the inequality of the flow field can be found in Bartholomay et al. (2017).

R1:Ma3.4-f **R2:Ma4-b** Table 5 gives an overview of some mean parameters characterizing the velocity plane $0.43d$ upstream of the rotor plane. In the experiment, the averaging was done over the measuring time, in the simulation over five revolutions. **R2:Ma4-c** The mean velocities in streamwise direction are slightly smaller than the desired velocity, both for

Table 5. Mean parameters for the velocity plane $0.43d$ upstream of the rotor plane.

	$\overline{u}$ [ms^{-1}]	$\overline{\sigma_u}$ [ms^{-1}]	$\overline{Ti}_{global}(uv)$ [%]
Measurement	6.42	$8.50 \cdot 10^{-2}$	1.20
FLOWer	6.47	—	—

measurement and simulation. However, as the differences are $< 0.5\%$ in the simulation and $\approx 1.23\%$ in the measurement, the reference velocity can still be considered as $6.5\mathrm{ms}^{-1}$. **R1:Ma2-i** **R2:Ma4-x** As uniform inflow was used in the present

simulation, the standard deviation and turbulence intensity are negligible. The turbulence intensity of the measurement corresponds to the value of the wind tunnel, which was already mentioned in subsection 2.2.1. The unsteady inflow in the experiment and the uniform inflow in the simulation lead to a discrepancy in the setups. However, the comparisons between measurement and calculation will be done anyway. The influence of the turbulence on the results will be discussed later in this document and **R1:Ma3.4-e** **R2:Ma7-f** reviewed in future investigations.

In Fig. 9, the relative difference between simulation and measurement with regard to the mean inflow velocity of $6.5\mathrm{ms}^{-1}$ is shown.

The differences between both velocity planes are small **R2:Ma4-d** **R1:Ma3.4-h** as the average deviation amounts 3.06%.

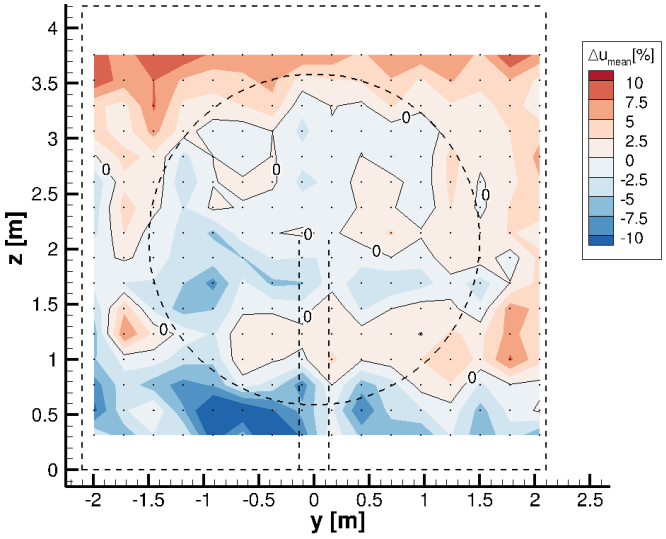

Figure 9. Relative velocity difference between measurement and simulation with regard to the undisturbed reference inflow velocity of $6.5\mathrm{ms}^{-1}$, $0.43d$ upstream of the rotor plane. The dashed lines illustrate the wind tunnel and the turbine. Isolines show 0% deviation. The dots show the discrete evaluation points.

Except for a small area at the bottom of the wind tunnel (**R1:G3** around $z = 0.5\mathrm{m}$ and between $-1\mathrm{m} < y < 0\mathrm{m}$), the **Authors** difference is lower than $\pm 10\%$ of the **Authors** desired inflow velocity, which corresponds to $\pm 0.65\mathrm{ms}^{-1}$.

Fig. 10 shows the velocity in x-direction $0.5d$ downstream of the rotor plane, for the measurement (left) and for the simulation (right). Again, the measuring points are indicated by black dots, the dimensions of the wind tunnel and the model wind turbine by dashed lines. An isoline with the mean velocity of $6.5\mathrm{ms}^{-1}$ is shown, too.

Some aspects, as already seen upstream of the rotor (Fig. 8) are apparent downstream of the rotor, **Authors** too. **R1:Mi29** For example the higher velocity over the ceiling in the measurement. Or the smoother, axisymmetric streamwise velocity in the simulation. In both figures (left and right), the wake of the rotor, indicated by lower velocity, can be seen clearly. Around the rotor, as a result of limited space due to the wind tunnel walls, higher velocities are achieved. Again, in the experiment, the velocity at the upper part of the wind tunnel is slightly higher than at the bottom.

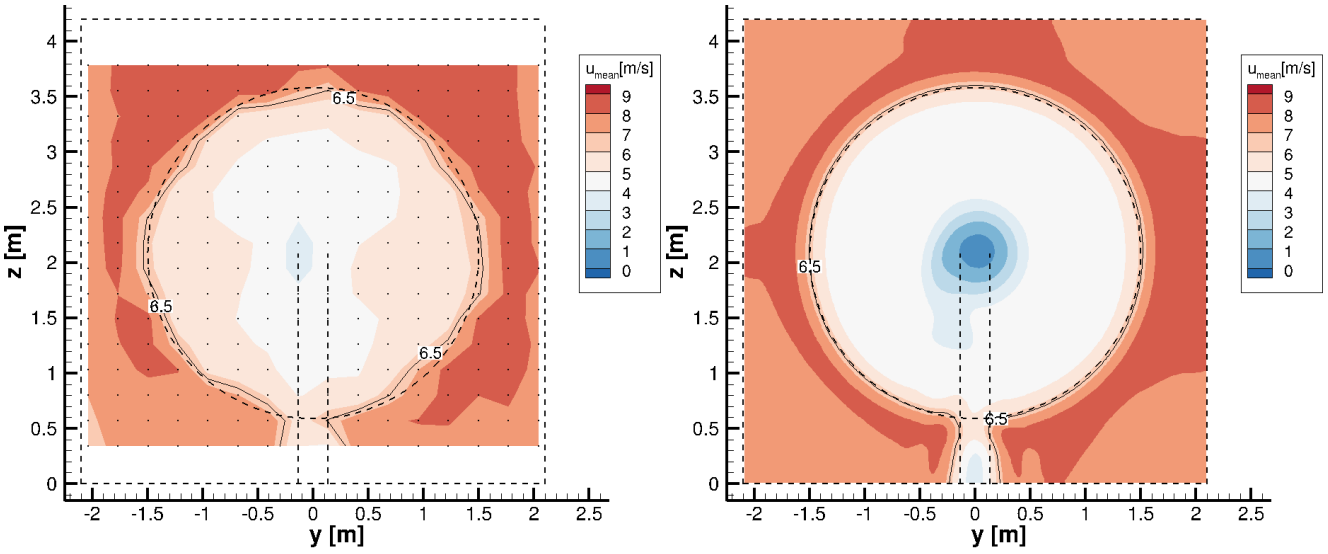

Figure 10. Hot-wire measurements (left) and simulated velocity plane (right) of the x-velocity $0.5d$ downstream of the rotor plane. The dashed lines illustrate the wind tunnel and the turbine. Isolines show the mean inflow velocity of $6.5\mathrm{ms}^{-1}$. The dots in the left figure show the discrete measuring points.

This missing turbulence in **R1:Mi30-b** the simulated wind tunnel **R1:Ma3.4-j** is the reason why the border of the rotor wake is almost a perfect circle in the right picture, whereas it is more smeared in the measurement. The decay of the tip vortices has not yet started so shortly behind the rotor plane. As the simulation has a finer resolution, the velocity distribution is smoother there. In the simulation, there is a stronger velocity deficit in the wake of the nacelle. This can have several reasons. **R1:Ma3.4-k** In the simulation, the missing inflow turbulence might have a small effect on the stability of the wake, but is certainly not the main reason for the deviation, see Medici and Alfredsson (2006). In the experiment, the boundary layer of the nacelle is not tripped, whereas a fully turbulent approach is used in the simulation. These differences concerning the boundary layer of the nacelle might lead to a different recovery of the wake of the nacelle. Due to the flow separation on the nacelle, the flow in the wake of the nacelle is highly unsteady and the main flow direction is not clearly defined (angles larger than $\pm 60°$ occur in the simulation), whereby proper working conditions of the x-wire probe are no longer guaranteed. Therefore, the measured x-component of the velocity is influenced by the y- and z-component, which could also lead to deviations between measurement and simulation.

R1:Ma3.4-g **R2:Ma4-e** An overview of some mean parameters characterizing the velocity plane $0.5d$ downstream of the rotor plane are given in Table 6.

R2:Ma4-f Again, the mean velocity almost corresponds to the desired reference velocity, as the differences between the actual velocity and $6.5\mathrm{ms}^{-1}$ are $< 0.5\%$ both for measurement and simulation. Due to the closed wind tunnel and the mass continuity, bigger differences would not have been physical. As the tip and root vortices, as well as the separation behind the nacelle, lead to velocity fluctuations, **R1:Ma2-j** **R2:Ma4-z** the standard deviation, as well as the turbulence intensity,

Table 6. Mean parameters for the velocity plane $0.5d$ downstream of the rotor plane.

	$\overline{u}$ [ms^{-1}]	$\overline{\sigma_u}$ [ms^{-1}]	$\overline{Ti}_{global}(uv)$ [%]
Measurement	6.53	$6.76 \cdot 10^{-1}$	7.01
FLOWer	6.48	$3.17 \cdot 10^{-1}$	3.71

increase compared to the plane upstream to the rotor, see Table 5. **Authors** Through the superposition of the vortices created by the turbine and the inflow turbulence, the values for the measurement are still larger. As the present wind tunnel is a circuit wind tunnel, effects like pumping might occur. And due to the long measurement time of the hot wire probes, these fluctuations might also be included in the values shown in Table 6.

Fig. 11 shows the relative difference between simulation and measurement with regard to the mean inflow velocity of 6.5ms^{-1}. **R1:Ma6-a** It can be seen that in the wake of the nacelle and in the area of the tip vortices, the differences between simulation

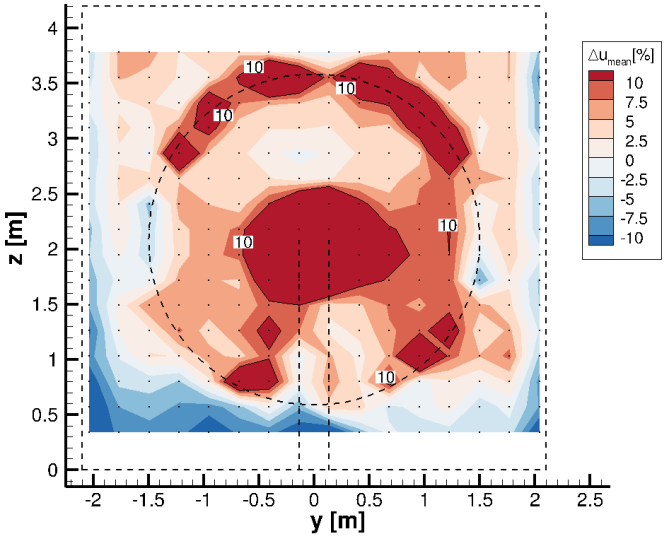

Figure 11. Relative velocity difference between measurement and simulation with regard to the undisturbed reference inflow velocity of 6.5ms^{-1}, $0.5d$ downstream of the rotor plane. The dashed lines illustrate the wind tunnel and the turbine. Isolines show 10% deviation. The dots show the discrete evaluation points.

and measurement are higher that 10%. In the remaining part, the difference is smaller. **R1:Ma3.4-i** **R2:Ma4-g** The mean deviation amounts 7.31%, which is considerably higher than the value for the plane upstream of the turbine. The reason for the high value is primary the area in the wake of the nacelle, where differences $> 50\%$ occur. If a circular area with a radius $r < 0.56\text{m}$ and its origin at the center of the rotor is neglected in the averaging, the mean deviation reduces to 5.90% as the mean deviation in this area itself amounts 31.22%. Thereby it has to be kept in mind, that due to the large flow angles in the

wake of the nacelle, the measured values in this area have to be treated with caution.

All things considered, the accordance between experiment and simulation is **R2:Ma4-bb** **R1:Ma6-b** acceptable, as the differences are, except for some parts in the outer region of the rotor and in the wake of the nacelle, smaller than $\pm 0.65\mathrm{ms}^{-1}$.

4.2 Analysis of the on-blade velocity

Hereinafter, the on-blade velocity, meaning the velocity seen by the blade section at a distinct radial position, for $CaseBASE$ for experiment, *QBlade* and *FLOWer* (both methods *RAV* and *CircAve*) are displayed at two different rotor locations (**R1:Mi31-a** $65\%R$ and $85\%R$) over the azimuth (Fig. 12). **R1:Mi31-b** A radius of $0\%R$ corresponds to the rotor center, whereas an azimuth of $0°$ corresponds to the top position of the first blade .

Authors At 65%R, the simulations overestimate the velocity, at 85%R there is a better accordance between the simulation

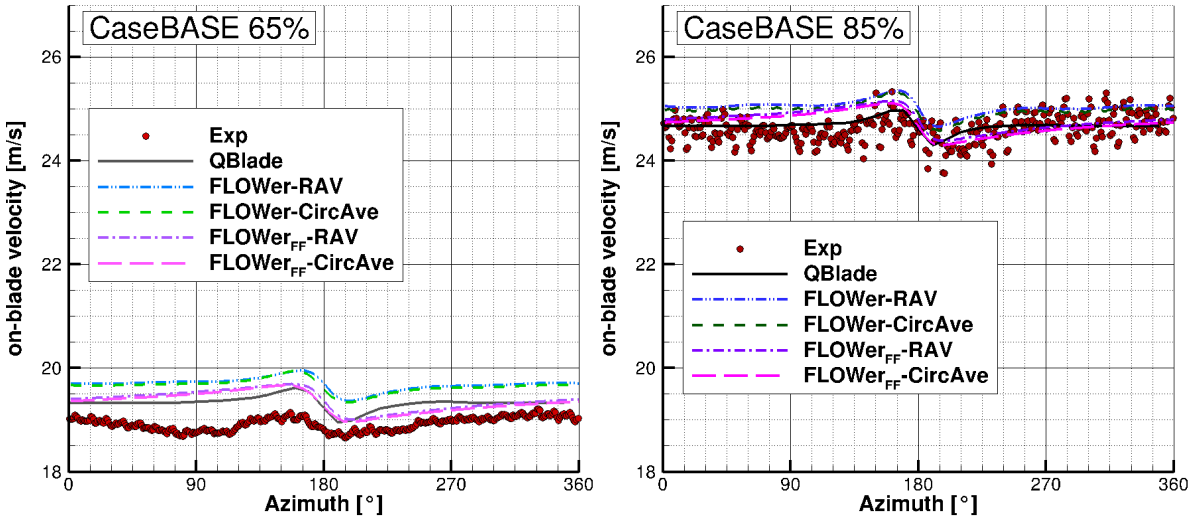

Figure 12. On-blade velocity distribution over azimuth for $CaseBASE$ for the experiment, *QBlade* and *FLOWer* (*RAV* and *CircAve* for wind tunnel and FF each) at $65\%R$ (left) and $85\%R$ (right).

results and the experiment. **R1:Ma3.4-l** The difference caused by the different inflow turbulence is even less pronounced at the on-blade velocity compared to the velocity planes, as the rotational velocity has a much higher influence than the inflow velocity. Therefore, the fluctuations in the measurements are not so distinct and the differences between measurement and simulation caused by the inflow turbulence are small. For their cases with and without free stream turbulence, Medici and Alfredsson (2006) also experienced only small differences in the drag coefficient, which depends on the angle of attack and consequently also on the on-blade velocity. **R2:Ma2-h** The higher fluctuations in the experiment at the outer radial position might be a result of a vibration of the mounting of the probe. **R1:Ma2-c** **R2:Ma4-s** The averaged standard deviation for the measured velocity amounts $\sigma_{on-blade}(65\%R) = 0.11\mathrm{ms}^{-1}$ and $\sigma_{on-blade}(85\%R) = 0.08\mathrm{ms}^{-1}$.

R2:Ma5-a In order to better assess the quantitative differences between the curves, Table 7 gives an overview of the relative differences between experiment and the different simulation results of the averaged on-blade velocity ($\Delta\overline{v} = \overline{v_{Sim}} - \overline{v_{Exp}}$) for $CaseBASE$ at both probe positions.

R2:Ma5-b The reference velocity in each case is the undisturbed velocity at the probe position, which was calculated with

$$v_{Ref} = \sqrt{{v_{inflow}}^2 + (\omega \cdot R)^2}. \tag{2}$$

R2:Ma5-c and amounts $v_{Ref}(65\%R) = 19.49\mathrm{ms}^{-1}$, respectively $v_{Ref}(85\%R) = 24.90\mathrm{ms}^{-1}$.

For both radial positions, all simulations match **R2:Ma5-d** fairly well to each other, as the differences to the experiment are

Table 7. Relative differences between the experiment and the different simulation results of the averaged on-blade velocity with respect to the undisturbed velocity at the probe positions for $CaseBASE$.

$\Delta\overline{v}$ [%]	*QBlade*	*FLOWer* $- RAV$	*FLOWer* $- CircAve$	*FLOWer*$_{FF} - RAV$	*FLOWer*$_{FF} - CircAve$
$65\%R$	2.05	3.90	3.72	2.31	2.10
$85\%R$	0.25	1.68	1.44	0.68	0.43

relatively similar. However, all simulations overestimate the experimental results. For the *FLOWer* simulations, both methods (*RAV* and *CircAve*) **R2:Ma5-e** show almost the same results ($\Delta\overline{v}_{FLOWer-RAV} = 3.90\%$ and $\Delta\overline{v}_{FLOWer-CircAve} = 3.72\%$ at $65\%R$ and $\Delta\overline{v}_{FLOWer-RAV} = 1.68\%$ and $\Delta\overline{v}_{FLOWer-CircAve} = 1.44\%$ at $85\%R$), whereby the CircAve method seems to fit better to the experimental results. In the outer part of the blade, **R2:Ma5-f** where the probes are located, the on-blade velocity is dominated by the tangential velocity. Consequently, both *FLOWer* setups (wind tunnel and far field), show almost the same results, too. **R2:Ma5-g** But due to the wind tunnel walls, the inflow velocity in the rotor plane is slightly higher than in the far field case, which can be seen in the marginal higher curves for the wind tunnel case.

With increasing radius, the difference between the wind tunnel and the far field case decreases, as the rotational part of the velocity becomes more and more dominant. The *QBlade* results are closest to the measured data, which is surprising, as the wind tunnel walls are not taken into account in the *LLFVW* simulations. Due to the lack of the walls, they have a better accordance with the *FLOWer* far field results than with the ones including the walls. **R2:Ma2-i** The influence of the tower blockage around an azimuth of $180°$ can be seen at both radial positions as a small increase before the tower passage and a small drop afterwards. The increase of the inflow velocity is due to the displacement effect of the tower. Directly upstream of the tower, the velocity is reduced until it has recovered shortly afterwards. Except for this drop, the velocity is almost constant over the whole revolution.

Fig. 13 shows the velocity over azimuth under yaw=$-15°$. As the wind tunnel walls should not be neglected in the present setup, a far field case under yawed condition for *FLOWer* was not simulated.

R1:Ma2-d **R2:Ma4-t** Under $15°$ yaw misalignment, the averaged standard deviation for the measured velocity is the same as for $CaseBASE$ ($\sigma_{on-blade}(65\%R) = 0.11\mathrm{ms}^{-1}$ and $\sigma_{on-blade}(85\%R) = 0.08\mathrm{ms}^{-1}$). **R2:Ma5-h** Table 8 gives an

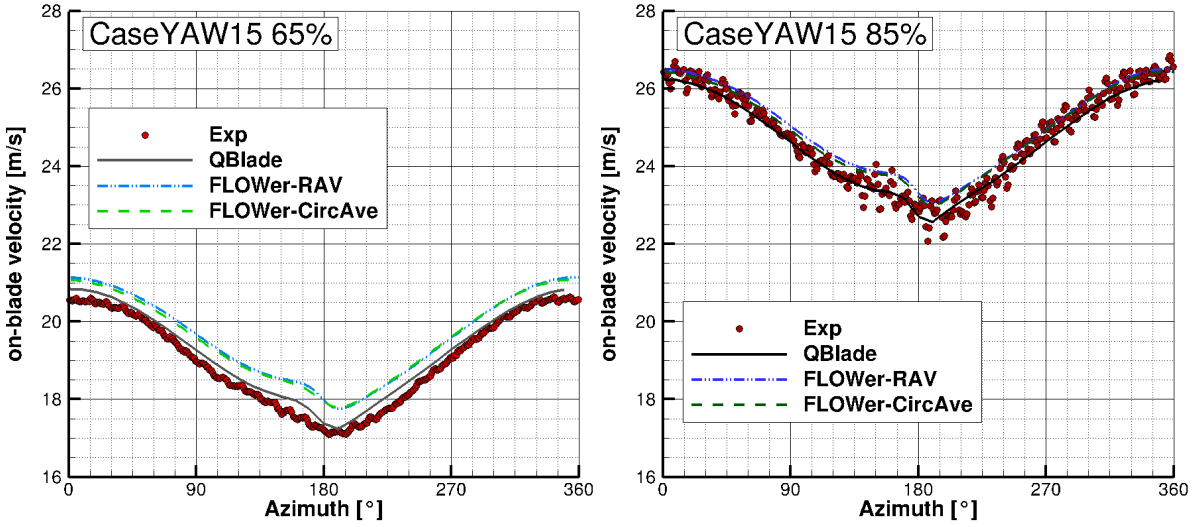

Figure 13. On-blade velocity distribution over azimuth for $CaseYAW15$ for the experiment, *QBlade* and *FLOWer* (*RAV* and *CircAve*) at $65\%R$ (left) and $85\%R$ (right).

overview of the relative differences between experiment and the different simulation results of the averaged on-blade velocity for $CaseYAW15$ at both probe positions.

At 65%R, the experimental and *QBlade* results are almost identical **R2:Ma5-i** ($\Delta\overline{v}_{QBlade} = 0.96\%$), whereas *FLOWer* predicts a slightly higher velocity ($\approx 0.5\mathrm{ms}^{-1}$, **R2:Ma5-j** which corresponds to $\Delta\overline{v}_{FLOWer} \approx 3\%$). At 85%R, there is still a small offset between *QBlade* and *FLOWer*, but the measurement lies between the two curves, **R2:Ma5-k** which can also be seen at the different signs of the differences in Table 8. Moreover, as already seen for the case with no yaw misalignment, the differences are smaller further outboard. In total, the differences between experiment and simulations are smaller than under straight inflow.

Table 8. Relative differences between the experiment and the different simulation results of the averaged on-blade velocity with respect to the undisturbed velocity at the probe positions for $CaseYAW15$.

$\Delta\overline{v}$ [%]	*QBlade*	$FLOWer - RAV$	$FLOWer - CircAve$
$65\%R$	0.96	3.04	2.87
$85\%R$	-0.54	1.05	0.82

The influence of the tower is covered by the influence of the yaw misalignment, which leads to stronger variations over one revolution. In the upper part of the rotor (azimuth=270°-90°), the blade is advancing, while it is retreating in the lower part (azimuth=90°-270°). This leads to a $1p$ variation of inflow velocity as seen by the blade. **R1:Mi32** Further information and

detailed discussions about effects occurring under yaw misalignment, like the $1p$ variation, are summarized by Schulz et al. (2017).

In Fig. 14, where the velocity over azimuth under yaw=$-30°$ is plotted, the influence of the yaw misalignment is even more pronounced.

R1:Ma2-e **R2:Ma4-u** Again, the averaged standard deviation for the measured velocity amounts $\sigma_{on-blade}(65\%R) = 0.11\text{ms}^{-1}$

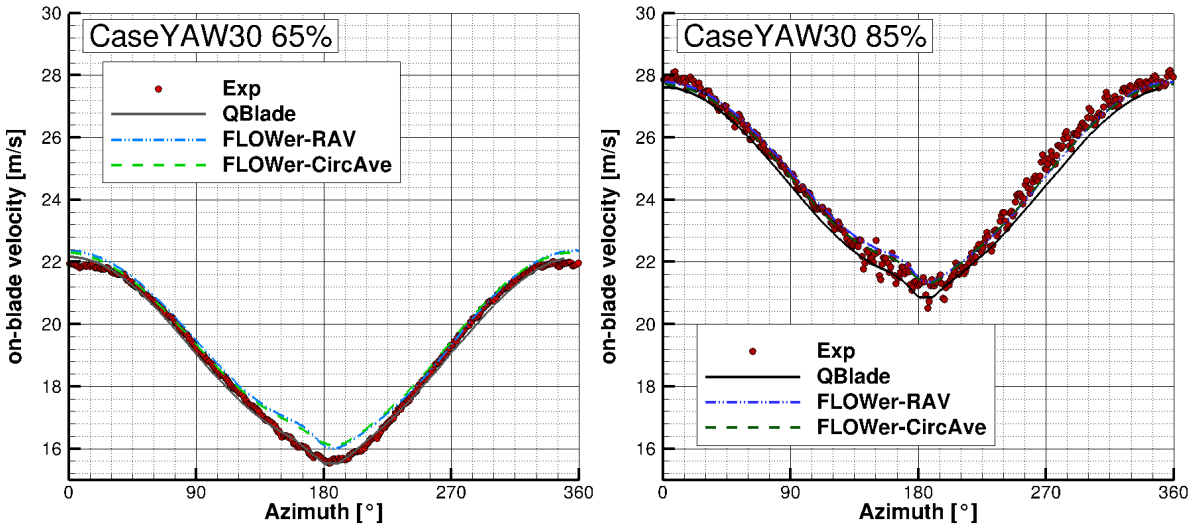

Figure 14. On-blade velocity distribution over azimuth for $CaseYAW30$ for the experiment, *QBlade* and *FLOWer* (*RAV* and *CircAve*) at $65\%R$ (left) and $85\%R$ (right).

and $\sigma_{on-blade}(85\%R) = 0.08\text{ms}^{-1}$. **R2:Ma5-l** In Table 9, the relative differences between experiment and the different simulation results of the averaged on-blade velocity for $CaseYAW30$ at both probe positions are displayed.

Almost the same characteristics as already mentioned with regard to Fig. 13 can be found for $-30°$ yaw misalignment. However, at 65%R, the *FLOWer* results have a better agreement with the experiment in the upper part of the rotor **R2:Ma5-m** (270° to 90° azimuth) than in the lower part (90° to 270° azimuth). At 85%R the *FLOWer* curves and the measured curve correspond well ($|\Delta\overline{v}_{FLOWer}| \leq 0.11\%$, whereas the *QBlade* results have a bigger deviation to the experimental results. Overall,

Table 9. Relative differences between the experiment and the different simulation results of the averaged on-blade velocity with respect to the undisturbed velocity at the probe positions for $CaseYAW30$.

$\Delta\overline{v}$ [%]	*QBlade*	*FLOWer − RAV*	*FLOWer − CircAve*
$65\%R$	-0.79	1.41	1.30
$85\%R$	-1.65	0.11	-0.1

the differences between the simulated curves and the measured curves decrease again with increasing yaw misalignment.

4.3 Evaluation of the angle of attack

As for the on-blade velocity, in the following, the AoA for $CaseBASE$ for experiment, *QBlade* and *FLOWer* (both methods *RAV* and *CircAve*) are displayed at two different rotor locations (65% and 85%) over the azimuth (Fig. 15).

The tower blockage effect can be clearly seen at azimuth=$180°$, where the AoA has a drop of approximately $1°$. The influence

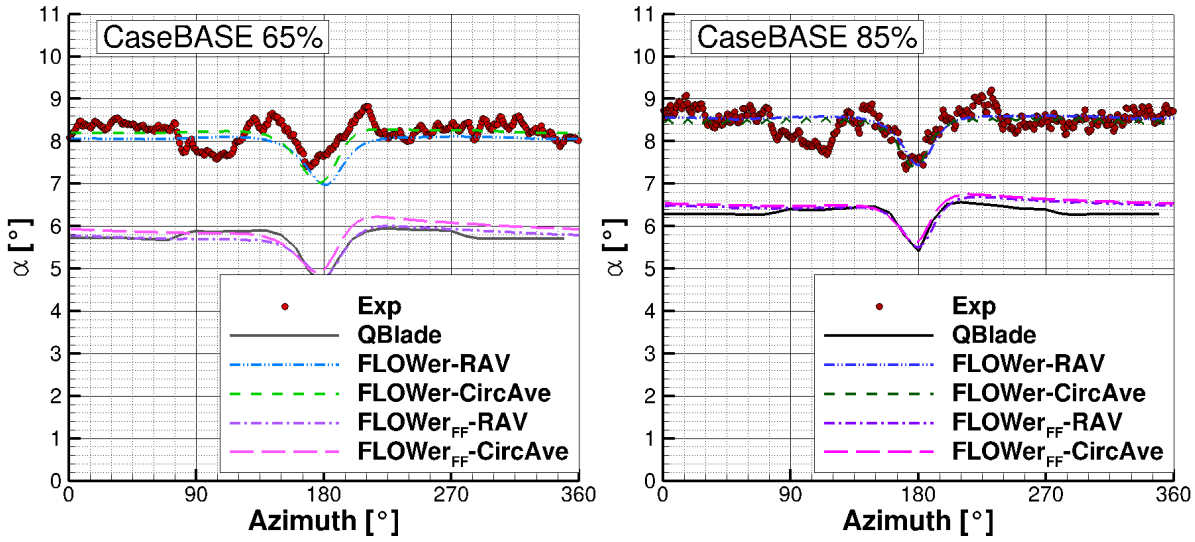

Figure 15. AoA distribution over azimuth for $CaseBASE$ for the experiment, *QBlade* and *FLOWer* (*RAV* and *CircAve* for wind tunnel and FF each) at $65\%R$ (left) and $85\%R$ (right).

of the tower is very distinct, due to its relative large diameter, compared to the other components of the turbine. For both, *QBlade* and *FLOWer*, the curve is almost constant before and after this drop. The dip in the experiment at approximately $90°$ azimuth is a result from the traverse, which was located in the test section upstream of the rotor.

R2:Ma5-n Table 10 gives an overview of the differences between experiment and the different simulation results of the averaged angle of attack ($\Delta\overline{\alpha} = \overline{\alpha_{Sim}} - \overline{\alpha_{Exp}}$) for $CaseBASE$ at both probe positions in order to quantify them. In contrast to the on-blade velocity, no relative values were calculated.

There is a good accordance between the experiment and the *FLOWer* results **R1:Ma2-f** **R2:Ma4-h** despite the fact that the simulated curves lie outside of the measured standard deviation whose average is however small ($\sigma_\alpha(65\%R) = 0.10°$ and $\sigma_\alpha(85\%R) = 0.14°$). Though, they are within the range of the maximum absolute error of $0.8°$, compare subsection 3.2. The larger value for the more outboard region mirrors the effect of the vibrating mounting of the probe. Both AoA evaluation methods for the *FLOWer* solution show almost the same distribution, especially at 85% **R2:Ma5-o** ($|\Delta\overline{\alpha}_{FLOWer}| \leq 0.23°$ at 65%R and $|\Delta\overline{\alpha}_{FLOWer}| \leq 0.03°$ at 85%R). Reasons for the differences can be attributed to the different approach of the

Table 10. Differences between the experiment and the different simulation results of the angle of attack for $CaseBASE$.

$\Delta\overline{\alpha}$ [°]	*QBlade*	$FLOWer - RAV$	$FLOWer - CircAve$	$FLOWer_{FF} - RAV$	$FLOWer_{FF} - CircAve$
$65\%R$	-2.48	-0.23	-0.08	-2.48	-2.33
$85\%R$	-2.13	0.03	-0.03	-2.00	-1.95

methods (*RAV* is averaging over time and *CircAve* has a local approach, **R1:Mi33** see Jost et al. (2018)). At 65%, the level of the AoA is approximately $0.5°$ lower than further outboard for experiment, *QBlade* and *FLOWer*.

R2:Ma5-p An offset of $> 2°$ between the simulation results of *QBlade* and *FLOWer* **Authors** (including wind tunnel walls) is present for both radial positions. **R2:Ma2-i** This is a result of the neglection of the wind tunnel walls in the *QBlade* simulation. A comparison between the *QBlade* results and the *FLOWer* results under far field condition verifies this assumption, as both the distributions, **R2:Ma5-q** and the offsets to the measured values, see Table 10, are almost similar. **R2:Ma5-aa** The small kinks at $\approx 90°$ and $\approx 270°$ azimuth in the *QBlade* results are a result of the usage of the tower model. This model has to be switched on at a certain blade position. In the present simulations this is done as soon as the blade position is located below the nacelle, leading to a discontinuity, which is reduced through interpolation. However, as the tower has a relatively large diameter, the kink can't be completely prevented.

A comparison of the AoA distribution calculated by *QBlade* and *FLOWer* over the normalized radius at azimuth=$0°$ for the wind tunnel and far field cases is shown in Fig. 16.

Again, the influence of the wind tunnel can be seen in the constant offset between the two *FLOWer* cases. As already seen in Fig. 15 **R2:Ma5-r** and Table 10, the offset between the *RAV* and the *CircAve* results amounts $\approx 0.15°$ **R2:Ma5-s** at 65%R and decreases to $\approx 0.06°$ at 85%R for both cases (far field and wind tunnel). As already mentioned, the differences are a result of the different approaches of the two methods, see Jost et al. (2018). Between approximately 40% and 90% of the radius, there is a good accordance between the *QBlade* and the *RAV* solution of the *FLOWer* far field case.

Fig. 17 shows the AoA over azimuth under yaw=$-15°$.

The same characteristics as under yaw=$0°$ can also be seen in Fig. 17 under yaw=$-15°$. Again, the influences of the tower blockage **R1:Ma7-a** and the traverse are clearly visible. Unlike in $CaseBASE$, the AoA is not constant before and after the drop caused by the tower, due to the yaw misalignment.

R2:Ma5-t In Table 11, an overview of the differences between experiment and the different simulation results of the averaged angle of attack for $CaseYAW15$ at both probe positions is given.

As in $CaseBASE$, the *FLOWer* results show a good agreement to the measurements at both radial positions **R2:Ma5-u** ($|\Delta\overline{\alpha}_{FLOWer}| \leq 0.18°$ at 65%R and $|\Delta\overline{\alpha}_{FLOWer}| \leq 0.13°$ at 85%R) **R1:Ma2-g** **R2:Ma4-v** and the average of the measured deviation is again small and similar the to values for the $CaseBASE$ ($\sigma_\alpha(65\%R) = 0.10°$ and $\sigma_\alpha(85\%R) = 0.14°$). Again, the differences of the *CFD* results including wind tunnel are smaller than the maximal absolute error of $0.8°$. The two different evaluation methods for *FLOWer* show almost the same results, too. The difference between the two radial positions

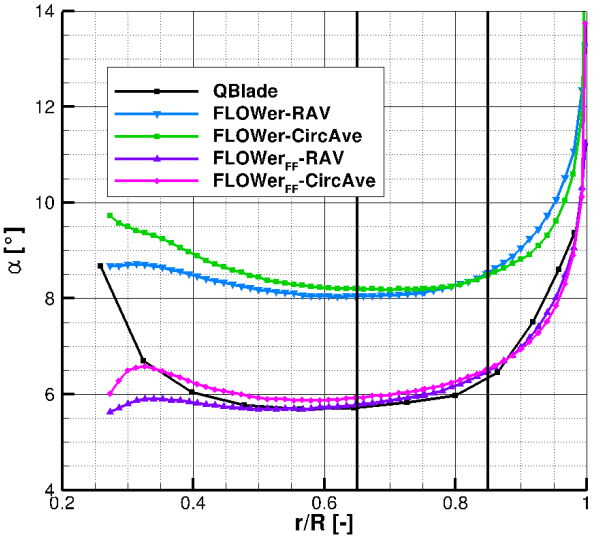

Figure 16. AoA distribution over the normalized blade radius at azimuth=0° for *QBlade* and *FLOWer* (*RAV* and *CircAve* for wind tunnel and FF each). Black lines indicate the evaluation positions of Fig 15, Fig 17 and Fig 18.

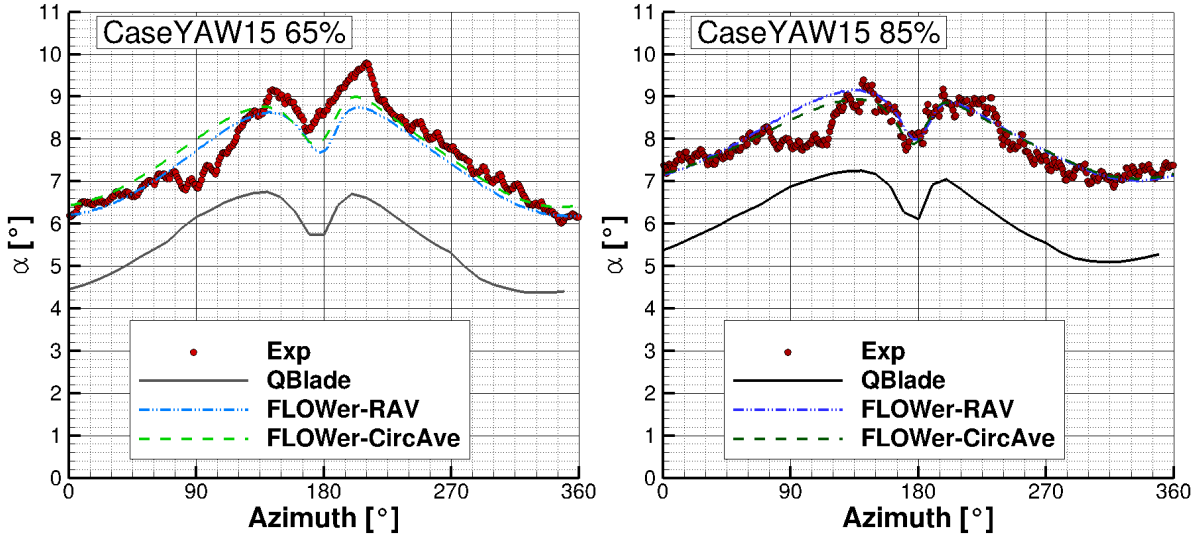

Figure 17. AoA distribution over azimuth for $CaseYAW15$ for the experiment, *QBlade* and *FLOWer* (*RAV* and *CircAve*) at $65\%R$ (left) and $85\%R$ (right).

amounts approximately 1° for all setups. The offset between *QBlade* and *FLOWer* **R2:Ma5-v** is $> 1.8°$ and but smaller than for case $CaseBASE$ but can still be attributed to the influence of the wind tunnel walls. **R2:Ma5-bb** The reduction of the difference between *QBlade* and *FLOWer* is a result of the yaw misalignment. Through the rotation of the rotor plane out of the

Table 11. Differences between the experiment and the different simulation results of the angle of attack for $CaseYAW15$.

$\Delta\overline{\alpha}$ [°]	*QBlade*	*FLOWer* − *RAV*	*FLOWer* − *CircAve*
$65\%R$	-2.05	-0.18	0.01
$85\%R$	-1.76	0.13	0.07

inflow plane, the projected plane gets smaller, leading to a smaller blockage in the wind tunnel. As the change of the projected area follows the cosine-function, the changes in the differences are not linear. As already mentioned, a far field case under yaw misalignment for *FLOWer* was not simulated. **Authors** The kinks at $\approx 90°$ and $\approx 270°$ azimuth are still present, but less pronounced.

In Fig. 18 the AoA distribution over azimuth for a yaw misalignment of $-30°$ can be seen.

The effects of the tower blockage **R1:Ma7-b** and the traverse are still visible. The effects caused by the yaw misalignment

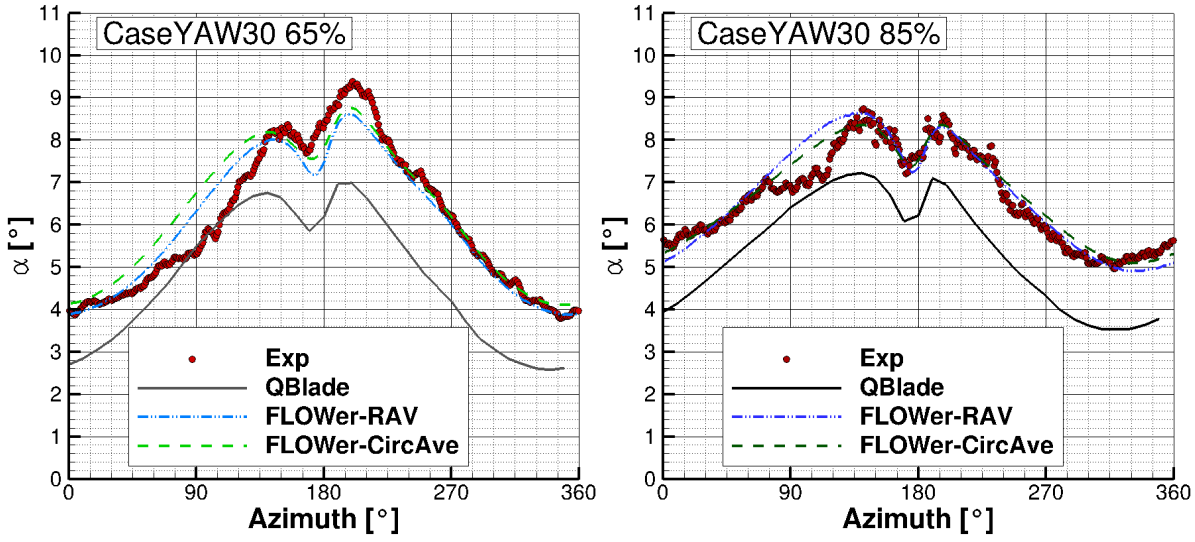

Figure 18. AoA distribution over azimuth for $CaseYAW30$ for the experiment, *QBlade* and *FLOWer* (*RAV* and *CircAve*) at $65\%R$ (left) and $85\%R$ (right).

are more pronounced here.

R2:Ma5-w An overview of the differences between experiment and the different simulation results of the averaged angle of attack for $CaseYAW30$ at both probe positions is given in Table 12.

At 65%, there is a difference between the measurement and *FLOWer* results at the downward moving blade (azimuth=0°-180°), probably due to the traverse placed in the wind tunnel, whereas there is a good agreement at the upward moving blade (azimuth=180°-360°). **R2:Ma5-x** The average accordance between the experiment and the *FLOWer* simulations is satisfac-

Table 12. Differences between the experiment and the different simulation results of the angle of attack for $CaseYAW30$.

$\Delta\overline{\alpha}$ [°]	*QBlade*	*FLOWer* − RAV	*FLOWer* − $CircAve$
$65\%R$	−1.32	−0.02	0.23
$85\%R$	−1.25	0.11	0.12

tory, as the differences are small ($|\Delta\overline{\alpha}_{FLOWer}| \leq 0.23°$). Further outboard, the curves correspond very well over the whole revolution **R2:Ma5-y** ($|\Delta\overline{\alpha}_{FLOWer}| \leq 0.12°$), except for the dip at 90° azimuth. **R1:Ma2-h** **R2:Ma4-w** The average of the deviation amounts $\sigma_\alpha(65\%R) = 0.09°$ and $\sigma_\alpha(85\%R) = 0.13°$, which can be considered as small. The offset between *QBlade* and *FLOWer*, due to the missing wind tunnel walls in *QBlade*, has decreased and amounts now **R2:Ma5-z** $< 1.6°$. For all three cases ($CaseBASE$, $CaseYAW15$ and $CaseYAW30$) at both radial positions, despite the constant offset to the *QBlade* results, the amplitude and phase of the AoA of experiment, *QBlade* and *FLOWer* have a good agreement.

4.4 Investigation of the bending moments

R1:Ma8-e **R2:Ma2-e** In the following, the flapwise bending moments (out-of plane, M_y) for one blade, simulated with *QBlade* and *FLOWer*, are compared to each other for all three cases. Fig. 19 shows the curves for $CaseBASE$ (upper left), $CaseYAW15$ (upper right) and $CaseYAW30$ (lower middle).

As the forces and moments mainly depend on the AoA, the same characteristics (tower shadow, influence of yaw misalignment,...) like in Fig. 15, Fig. 17 and Fig. 18, can be seen in Fig. 19, as they cascade down from the AoA to the loads.

R2:Ma4-i In Table 13, the relative differences between the simulation results of the flapwise bending moment are displayed. The **Authors** difference between the two *FLOWer* results for the baseline case (upper left figure, **R2:Ma4-j** 19.64%) represents the influence of the wind tunnel walls. However, this time, the accordance between the *QBlade* results and the *FLOWer* wind tunnel case **R2:Ma4-k** (8.87%) is slightly better than between the *QBlade* case and the *FLOWer* far field case. This un-

Table 13. Relative differences between the different simulation results of the averaged flapwise bending moment with respect to the *FLOWer* solution including wind tunnel walls.

$\Delta\overline{M_y}$ [%]	*QBlade*	*FLOWer*$_{FF}$
$CaseBASE$	8.87	19.64
$CaseYAW15$	7.86	—
$CaseYAW30$	2.81	—

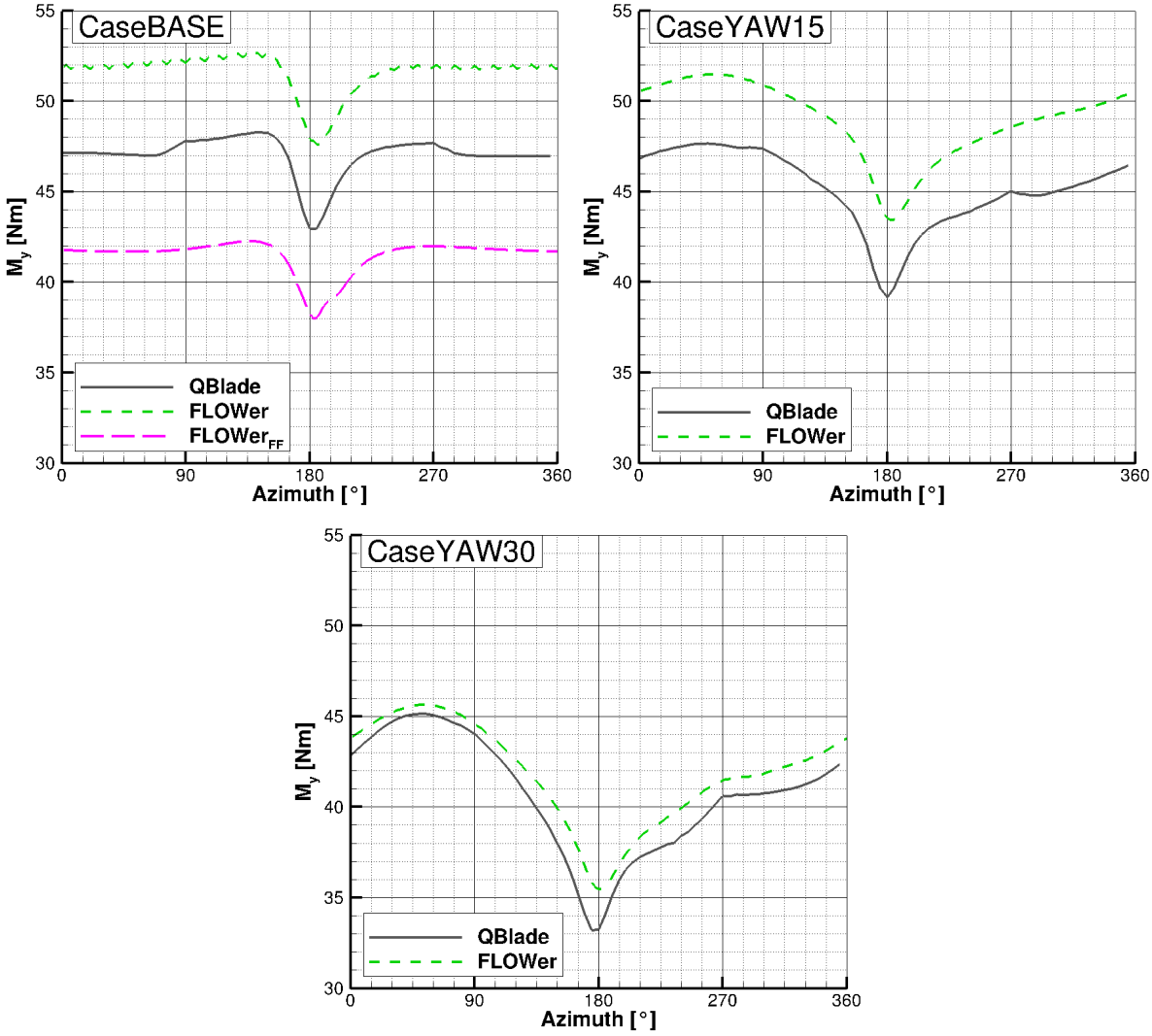

Figure 19. Simulated flapwise bending moment (M_y) over azimuth for $CaseBASE$ (upper left), $CaseYAW15$ (upper right) and $CaseYAW30$ (lower middle) for *QBlade* and *FLOWer*.

expected result might be a result of the choice of the *XFOIL* polars used for the present *QBlade* simulations, because although the AoA are similar between *QBlade* and $CaseBASE_{FLOWer-FF}$ (see Fig. 15 **R2:Ma4-l** and Table 10), the bending moments differ. Comparisons of the radial moment distribution and of the force coefficient over the azimuth could lead to a better understanding and assessment of the differences.

The amplitude and phase of the $1p$ frequency, caused by the yaw misalignment, show a good accordance between **R1:Ma8-f** *QBlade* and *FLOWer* for $CaseBASE$ and $CaseYAW15$. **R2:Ma4-m** The mean differences under yaw misalignment decrease with increasing yaw angle (7.86% under 15° yaw misalignment and 2.81% under 30° yaw misalignment), showing the

same tendency as the angle of attack (Table 10, Table 11 and Table 12). **Authors** Except for the constant offset, the fit between the curves of the *QBlade* and *FLOWer* simulations is similar to the one for the on-blade velocity and the angle of attack. This time, the kinks in the curves at $\approx 90°$ and especially at $\approx 270°$ are a bit more pronounced. For all three cases, *QBlade* predicts, due to the missing wind tunnel walls, smaller values than *FLOWer*.

The comparison of the edgewise bending moments (in plane, M_x) can be found in Fig. 20.

The same characteristics of the curves as for the flapwise bending moments (see Fig. 19) can be found in the **R1:Ma8-g**

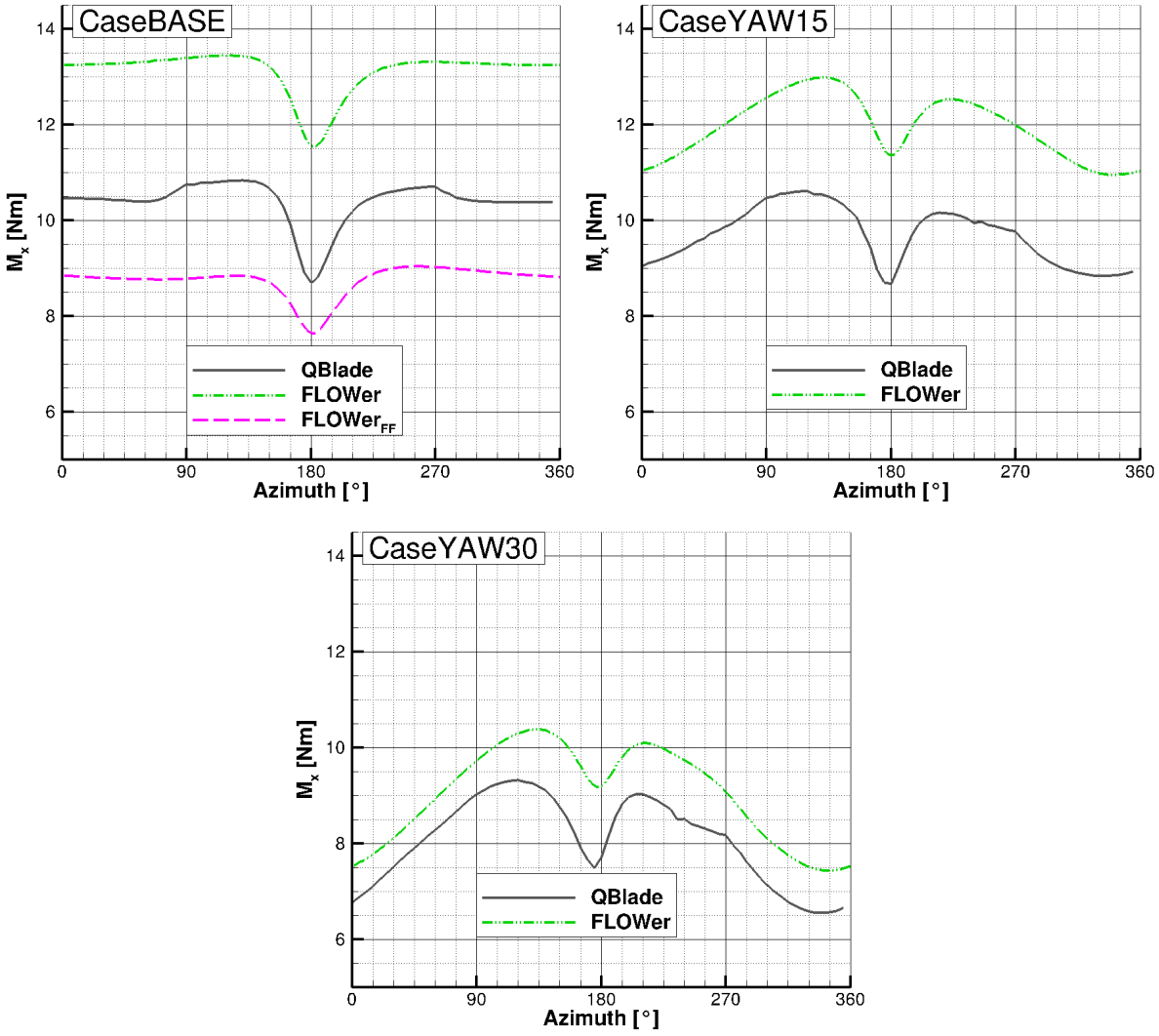

Figure 20. Edgewise bending moment (M_x) over azimuth for $CaseBASE$ (upper left), $CaseYAW15$ (upper right) and $CaseYAW30$ (lower middle) for experiment, *QBlade* and *FLOWer*.

simulated edgewise bending moments.

R2:Ma4-n The relative differences between the different simulation results for the edgewise bending moments are summarized in Table 14.

R2:Ma4-o The differences between the *FLOWer* results with and without wind tunnel walls are larger than for the flapwise

Table 14. Relative differences between the different simulation results of the averaged edgewise bending moment with respect to the *FLOWer* solution including wind tunnel walls.

$\Delta\overline{M_x}$ [%]	*QBlade*	*FLOWer*$_{FF}$
$CaseBASE$	20.82	33.37
$CaseYAW15$	19.04	—
$CaseYAW30$	10.67	—

bending moment ($\Delta\overline{M_x} = 33.37\%$ compared to $\Delta\overline{M_y} = 19.64\%$, see Table 13). This corresponds to the results of Fischer et al. (2018) and Klein et al. (2018), who also experienced a stronger influence of the walls on the power than on the thrust. The reason for this phenomenon might be the greater sensitivity of the tangential force, which is the main drive of the in plane moment, on the AoA compared to the normal force. Consequently, small differences in the AoA lead to larger deviations in F_T than in F_N. Other than for M_y, the *QBlade* results for M_x are closer to the *FLOWer* far field results than to the wind tunnel results. The progression of the edgewise bending moment is almost similar between *QBlade* and *FLOWer* for all three inflow directions. The mean differences under 15° yaw misalignment (19.04%) are slightly smaller than for $CaseBASE$ (20.82%), but the difference under 30° yaw misalignment is significantly smaller (10.67%) than for the other two cases. Again, the change in the projected area and the blockage in the wind tunnel can be alluded as reason for this tendency.

To sum up, the progression of the curves fit quite good for both moments, except the kinks caused by the tower shadow model in *QBlade*. The offset between the results seem to depend on to consideration of the wind tunnel walls and the chosen polar set in *QBlade*. The decreasing differences between *QBlade* and *FLOWer* with increasing yaw misalignment is a result of the decreasing projected rotor plane which influences the blockage in the wind tunnel.

5 Summary

Authors Experimental und numerical investigations of a model wind turbine, placed in a wind tunnel with high blockage ratio, were presented in the present paper. Thereby, two codes of different fidelity were used. In the simulations conducted with the Lifting Line Free Vortex Wake code *QBlade*, **R1:Ma10-t** the wind tunnel walls had to be neglected and the turbine was simulated under far field condition. **Authors** Unsteady Reynolds-averaged Navier-Stokes simulations have been performed with the Computational Fluid Dynamics code *FLOWer*. **R1:Ma10-u** Thereby, a far field case, as well as simulations including the wind tunnel walls, were investigated. In all simulations, the tower was considered, but they have been performed under uniform inflow, neglecting the turbulent inflow in the experiment.

Authors The experiments provided validation data and the comparison between experiment and the *FLOWer* wind tunnel case aimed at the validation of the *CFD* simulation. Through the comparison between two *FLOWer* cases (wind tunnel and far field) the influence of the blockage ratio was assessed. **R1:Ma1-d** **R2:Ma3-g** With the knowledge about the influence of the wind tunnel walls, the suitability of the *LLFVW* code to perform preliminary investigations for future studies with the model wind turbine could be investigated by a the comparison between *QBlade* and the *FLOWer* far field case.

Authors A comparison between the measured flow fields and the velocity planes extracted from *FLOWer* simulations including wind tunnel walls was conducted. Thereby, two different velocity planes were investigated. One is located $0.43d$ upstream of the turbine, one $0.5d$ downstream. **R1:Ma10-a** The velocity fields upstream of the turbine showed a good agreement in the rotor area, as the **R1:Ma10-b** **R2:Ma4-p** average deviation amounts 3.06% of the inflow velocity. **R1:Ma10-c** Downstream of the rotor plane, the differences were more pronounced **R1:Ma10-d** **R2:Ma4-q** (mean deviation 7.31% of the inflow velocity). **R1:Ma10-e** The areas of the tip vortices and the wake of the nacelle are most prominent. **R1:Ma10-g** The differences between the experimental and numerical results upstream and downstream are caused, amongst other, by vertical shear and higher turbulence in the measurements. Additionally, the differences in the wake of the nacelle and the outer region of the rotor might be caused by the high flow angles influencing the hot wire measurement downstream of the rotor.

Authors At two radial positions (65%R and 85%R), the on-blade velocity and the AoA were measured with 3-hole probes and compared to the results obtained from *QBlade* and both *FLOWer* cases. For the investigation of these parameters, three different yaw cases (yaw=$0°$; $-15°$ and $-30°$) were considered.

R1:Ma10-i The mean deviations of the on-blade velocity between the experiment and each simulation are $< 4\%$ at 65% of the radius and $< 2\%$ at 85% of the radius.

R1:Ma10-j The AoA calculated with *FLOWer* including wind tunnel showed a good agreement with the experimental results, as the maximum mean difference amounts $0.23°$. **Authors** As the *QBlade* results and the *FLOWer* simulation without wind tunnel walls are almost similar, the constant offset of approximately $1°$-$2°$ between the experiment and the far field simulations is a result of the neglection of the wind tunnel walls.

Finally, the blade root bending moments are compared between **R1:Ma8-h** **R2:Ma2-f** *QBlade* and the two *FLOWer* cases. For the out-of plane bending moment, the difference between the two *FLOWer* cases (far field and wind tunnel) **Authors** can be accredited to the influence of the wind tunnel walls. **R1:Ma10-h** The offset between the *QBlade* results and both *FLOWer* cases can not only be attributed to the influence of the wind tunnel walls. As the bending moments differ between the two far field cases despite the good accordance concerning the AoA, the chosen set of airfoil polars, which is used in the *QBlade* simulations, influences the loads. The accordance between the calculated amplitude and phase of **R1:Ma8-i** *QBlade* and *FLOWer* is good.

R1:Ma8-j The same conclusions as for the flapwise bending moment can be drawn for the edgewise bending moment. However, the relative deviations between the simulated curves of *QBlade* and *FLOWer* are larger.

To sum up, **R1:Ma10-n** a good accordance was achieved for the absolute values and the azimuthal distribution regarding the on-blade velocity and the AoA. **R1:Ma10-o** Consequently the numerical setup of *FLOWer* can be seen as validated in terms of these two parameters. **Authors** Concerning the velocity planes, differences between experiment and *FLOWer* occur but

can be explained. The comparison between the two *FLOWer* cases (with and without wind tunnel walls) showed, that in the present case, the wind tunnel leads to a constant offset between the curves for the on-blade velocity, the AoA and the bending moments. Regarding the *QBlade* results, the on-blade velocity, as well as the amplitude and phase of the AoA can be seen as validated by the experiment, too. As the AoA distribution of *QBlade* lies on the far field solutions of *FLOWer*, the differences in the mean values of the AoA can be attributed to the absence of wind tunnel walls in the *QBlade* predictions. **Authors** The offset between *QBlade* and *FLOWer* wind tunnel case regarding the bending moments is not only a result of the neglection of the walls, but is also influenced by the set of airfoil polars used in the *LLFVW* simulation.

In a next step, **R1:Ma10-s** in order to better match the experimental conditions, simulations with unsteady inflow, considering the measured shear and turbulence, will be performed. Moreover, experiments with passive and active load control will be performed and compared to simulations of both, *QBlade* and *FLOWer*. Thereby, *QBlade* will be used for dimensioning purposes of the flaps prior to the experiments. Afterwards, the most promising configurations will be investigated numerically on a full size turbine by *QBlade* and *FLOWer*, where the *LLFVW* code can be used for the preliminary design, and the *CFD* code for the closer look into the aerodynamic details.

Data availability. Measurement data and simulation results can be provided by contacting the corresponding author or Thorsten Lutz (lutz@iag.uni-stuttgart.de).

Competing interests. The authors declare that they have no conflict of interest.

Acknowledgements. All computational resources used for the *FLOWer* simulations were provided by the High Performance Computing Center Stuttgart (*HLRS*). The studies presented in this article have been funded by the *German Research Foundation* (*DFG*) and were performed in the course of the *DFG* PAK 780 project. **Authors** The authors want to thank the reviewers and the editor for their useful suggestions.

References

Bak, C., Madsen, H. A., and Johansen, J.: Influence from blade-tower interaction on fatigue loads and dynamics (poster), in: 2001 European Wind Energy Conference and Exhibition (EWEC'01), pp. 394–397, WIP Renewable Energies, 2001.

Bartholomay, S., Fruck, W.-L., Pechlivanoglou, G., Nayeri, C. N., and Paschereit, C. O.: Reproducible Inflow Modifications for a Wind Tunnel Mounted Research Hawt, in: ASME Turbo Expo 2017: Turbomachinery Technical Conference and Exposition, pp. V009T49A013–V009T49A013, American Society of Mechanical Engineers, https://doi.org/10.1115/GT2017-64364, 2017.

Bastankhah, M. and Porté-Agel, F.: A wind-tunnel investigation of wind-turbine wakes in yawed conditions, in: Journal of Physics: Conference Series, vol. 625, p. 012014, IOP Publishing, http://stacks.iop.org/1742-6596/625/i=1/a=012014, 2015.

Bastankhah, M. and Porté-Agel, F.: Wind tunnel study of the wind turbine interaction with a boundary-layer flow: Upwind region, turbine performance, and wake region, Physics of Fluids, 29, 065 105, https://doi.org/10.1063/1.4984078, 2017.

Bechmann, A., Sørensen, N. N., and Zahle, F.: CFD simulations of the MEXICO rotor, Wind Energy, 14, 677–689, 2011.

Benek, J. A., Steger, J. L., Dougherty, F. C., and Buning, P. G.: in: Chimera. A Grid-Embedding Technique., 1986.

Bossuyt, J., Howland, M. F., Meneveau, C., and Meyers, J.: Wind tunnel study of the power output spectrum in a micro wind farm, in: Journal of Physics: Conference Series, vol. 753, p. 072002, IOP Publishing, http://stacks.iop.org/1742-6596/753/i=7/a=072002, 2016.

Bossuyt, J., Howland, M. F., Meneveau, C., and Meyers, J.: Measurement of unsteady loading and power output variability in a micro wind farm model in a wind tunnel, Experiments in Fluids, 58, 1, https://doi.org/https://doi.org/10.1007/s00348-016-2278-6, 2017.

Castaignet, D., Barlas, T., Buhl, T., Poulsen, N. K., Wedel-Heinen, J. J., Olesen, N. A., Bak, C., and Kim, T.: Full-scale test of trailing edge flaps on a Vestas V27 wind turbine: active load reduction and system identification, Wind Energy, 17, 549–564, 2014.

Celik, I. B., Ghia, U., Roache, P. J., et al.: Procedure for estimation and reporting of uncertainty due to discretization in {CFD} applications, Journal of fluids {Engineering-Transactions} of the {ASME}, 130, https://doi.org/10.1115/1.2960953, 2008.

Chamorro, L. P. and Porté-Agel, F.: A wind-tunnel investigation of wind-turbine wakes: boundary-layer turbulence effects, Boundary-layer meteorology, 132, 129–149, https://doi.org/10.1007/s10546-009-9380-8, 2009.

Chen, T. and Liou, L.: Blockage corrections in wind tunnel tests of small horizontal-axis wind turbines, Experimental Thermal and Fluid Science, 35, 565–569, https://doi.org/10.1016/j.expthermflusci.2010.12.005, 2011.

Drela, M. and GILES, M.: Viscous-inviscid analysis of transonic and low Reynolds number airfoils, AIAA journal, 25, 1347–1355, 1987.

Drela, M. and Youngren, H.: Xfoil subsonic airfoil development system, Open source software available at http://web. mit. edu/drela/Public/web/xfoil, 2008.

Finn, E. J.: How to measure turbulence with hot-wire anemometers–a practical guide, Dantec, Dynamics, 2002.

Fischer, A., Flamm, A., Jost, E., Lutz, T., and Krämer, E.: Numerical Investigation of a Model Wind Turbine, in: New Results in Numerical and Experimental Fluid Mechanics XI, pp. 717–727, https://doi.org/10.1007/978-3-319-64519-3_64, 2018.

Gallant, T. and Johnson, D.: In-blade angle of attack measurement and comparison with models, in: Journal of Physics: Conference Series, vol. 753, p. 072007, IOP Publishing, 2016.

Hirai, S., Honda, A., and Kariromi, K.: Wind loads investigations of HAWT with wind tunnel tests and site measurements, Wind Power Asia, Beijing, 2008.

Howland, M., Bossuyt, J., Kang, J., Meyers, J., and Meneveau, C.: Wind tunnel measurements of wake structure and wind farm power for actuator disk model wind turbines in yaw, in: APS Division of Fluid Dynamics Meeting Abstracts, 2016.

Jameson, A.: Time dependent calculations using multigrid, with applications to unsteady flows past airfoils and wings, AIAA paper, 1596, 1991, 1991.

Jameson, A., Schmidt, W., Turkel, E., et al.: Numerical solutions of the Euler equations by finite volume methods using Runge-Kutta time-stepping schemes, AIAA paper, 1259, 1981, 1981.

Johansen, J. and Sørensen, N. N.: Aerofoil characteristics from 3D CFD rotor computations, Wind Energy, 7, 283–294, https://doi.org/10.1002/we.127, 2004.

Jost, E., Fischer, A., Lutz, T., and Krämer, E.: An investigation of unsteady 3D effects on trailing edge flaps, in: Journal of Physics: Conference Series, vol. 753, p. 022009, IOP Publishing, 2016.

Jost, E., Klein, L., Leipprand, H., Lutz, T., and Krämer, E.: Extracting the angle of attack on rotor blades from CFD simulations, Wind Energy, accepted for publication, 2018.

Klein, A., Zabel, S., Lutz, T., and Krämer, E.: About the Influence of Wind Tunnel Walls, Tower and Nozzle on the Performance of a Model Wind Turbine, in: High Performance Computing in Science and Engineering'17, pp. 339–353, Springer, 2018.

Klein, L., Lutz, T., and Krämer, E.: CFD analysis of a 2-bladed multi-megawatt turbine, in: 10th PhD Seminar on Wind Energy in Europe, pp. 47–50, 28-31 October 2014, Orléans, France, 2014.

Kowarsch, U., Öhrle, C., Keßler, M., and Krämer, E.: Aeroacoustic Simulation of a complete H145 Helicopter in descent flight, Journal of the American Helicopter Society, 61, 1–13, https://doi.org/10.4050/JAHS.61.042001, 2016.

Kroll, N., Rossow, C., Becker, K., and Thiele, F.: The MEGAFLOW project, Aerosp. Sci. Technol., 4, 223–237, https://doi.org/10.1016/S1270-9638(00)00131-0, 2000.

Marten, D., Pechlivanoglou, G., Nayeri, C., and Paschereit, C.: Integration of a WT Blade Design tool in XFOIL/XFLR5, in: 10th German Wind Energy Conference (DEWEK 2010), Bremen, Germany, Nov, pp. 17–18, 2010.

Marten, D., Lennie, M., Pechlivanoglou, G., Nayeri, C., and Paschereit, C.: Integration of an Unsteady Nonlinear Lifting Line Free Vortex Wake Algorithm in a Wind Turbine Design Framework, in: EWEA Annual Meeting, Paris, Nov, pp. 17–20, 2015.

Marten, D., Lennie, M., Pechlivanoglou, G., Nayeri, C. N., and Paschereit, C. O.: Implementation, optimization, and validation of a nonlinear lifting line-free vortex wake module within the wind turbine simulation code qblade, Journal of Engineering for Gas Turbines and Power, 138, 072 601, https://doi.org/10.1115/1.4031872, 2016.

Medici, D. and Alfredsson, P.: Measurements on a wind turbine wake: 3D effects and bluff body vortex shedding, Wind Energy, 9, 219–236, https://doi.org/10.1002/we.156, 2006.

Meister, K.: Numerische Untersuchung zum aerodynamischen und aeroelastischen Verhalten einer Windenergieanlage bei turbulenter atmosphärischer Zuströmung, Shaker Verlag, 2015.

Montgomerie, B.: Methods for Root Effects, Tip Effects and Extending the Angle of Attack Range to+-180°, with Application to Aerodynamics for Blades on Wind Turbines and Propellers, Swedish Defence Research Agency, 2004.

Nayeri, C. N., Vey, S., Marten, D., Pechlivanoglou, G., Paschereit, C. O., Huang, X., Meinke, M., Schöder, W., Kampers, G., Hölling, M., Peinke, J., Fischer, A., Lutz, T., Krämer, E., Cordes, U., Hufnagel, K., Schiffmann, K., Spiegelberg, H., and Tropea, C.: Collaborative Research on Wind Turbine Load Control under Realistic Tubulent Inflow Conditions, 12th German Wind Energy Conference (DEWEK 2015), Bremen, Germany, May, 2015.

Pechlivanoglou, G., Fischer, J., Eisele, O., Vey, S., Nayeri, C., and Paschereit, C.: Development of a medium scale research hawt for inflow and aerodynamic research in the tu berlin wind tunnel, 12th German Wind, 15, 2015.

Pedersen, M. M., Larsen, T. J., Madsen, H. A., and Larsen, G. C.: Using wind speed from a blade-mounted flow sensor for power and load assessment on modern wind turbines, Wind Energy Science, 2, 547, 2017.

Sarlak, H., Nishino, T., Martínez-Tossas, L., Meneveau, C., and Sørensen, J. N.: Assessment of blockage effects on the wake characteristics and power of wind turbines, Renewable Energy, 93, 340–352, https://doi.org/10.1016/j.renene.2016.01.101, 2016.

Saverin, J., Marten, D., Pechlivanoglou, G., Nayeri, C. N., and Paschereit, C. O.: Coupling of an Unsteady Lifting Line Free Vortex Wake Code to the Aeroelastic HAWT Simulation Suite FAST, in: Proc. ASME Turbo Expo, 2016a.

Saverin, J., Peukert, J., Marten, D., Pechlivanoglou, G., Paschereit, C. O., and Greenblatt, D.: Aeroelastic simulation of multi-MW wind turbines using a free vortex model coupled to a geometrically exact beam model, in: Journal of Physics: Conference Series, vol. 753, p. 082015, IOP Publishing, 2016b.

Sayed, M., Lutz, T., and Krämer, E.: Aerodynamic investigation of flow over a multi-megawatt slender bladed horizontal-axis wind turbine, Renewable Energies Offshore, 2015.

Schepers, J. and Snel, H.: Model experiments in controlled conditions, ECN Report: ECN-E-07-042, 2007.

Schepers, J. G.: Engineering models in wind energy aerodynamics: Development, implementation and analysis using dedicated aerodynamic measurements, Aerospace Engineering. Delft University of Technology, https://doi.org/10.4233/uuid:92123c07-cc12-4945-973f-103bd744ec87, 2012.

Schreck, S. J., Sørensen, N. N., and Robinson, M. C.: Aerodynamic structures and processes in rotationally augmented flow fields, Wind Energy, 10, 159–178, http://dx.doi.org/10.1002/we.214, 2007.

Schulz, C., Letzgus, P., Lutz, T., and Krämer, E.: CFD study on the impact of yawed inflow on loads, power and near wake of a generic wind turbine, Wind Energy, 20, 253–268, https://doi.org/10.1002/we.2004, 2017.

Schümann, H., Pierella, F., and Sætran, L.: Experimental investigation of wind turbine wakes in the wind tunnel, Energy Procedia, 35, 285–296, https://doi.org/10.1016/j.egypro.2013.07.181, 2013.

Simms, D., Schreck, S., Hand, M., and Fingersh, L.: NREL unsteady aerodynamics experiment in the NASA-Ames wind tunnel: a comparison of predictions to measurements, Tech. rep., National Renewable Energy Lab., Golden, CO (US), 2001.

Van Garrel, A.: Development of a wind turbine aerodynamics simulation module, Technical Report, ECN, 2003.

Vey, S., Marten, D., Pechlivanoglou, G., Nayeri, C., and Paschereit, C. O.: Experimental and Numerical Investigations of a Small Research Wind Turbine, in: 33rd AIAA Applied Aerodynamics Conference, June, pp. 1–9, American Institute of Aeronautics and Astronautics, Reston, Virginia, https://doi.org/10.2514/6.2015-3392, 2015.

Wendler, J., Marten, D., Pechlivanoglou, G., Nayeri, C., and Paschereit, C.: Implementation and Validation of an Unsteady Aerodynamics Model for Horizontal and Vertical Axis Wind Turbines Within the Simulation Tool QBlade, ASME Paper No. GT2016-57184, 2016.